Chapter-5
Results and Discussion

5.1. CHAPTER-5 (PART-1)

NOVEL COMPOUNDS SERIES-I

5.1.1. In silico studies

5.1.1.1.Docking Validation Studies

Validation experiments for molecular docking are conducted to ensure the reliability of the docking protocol in accurately predicting the binding conformation of ligands. For celecoxib/arachidonic acid, this involves comparing the re-docked pose with its experimentally determined co-crystallized pose in the active site of the target protein, such as COX-2/5-LOX (Figure 5.1). The co-crystallized pose, obtained from X-ray crystallography data (e.g., from the Protein Data Bank), serves as the reference structure. In the validation process, celecoxib is extracted and re-docked into the active site using a docking algorithm like Glide or AutoDock. The accuracy of the docking is assessed by calculating the root-mean-square deviation (RMSD) between the re-docked and co-crystallized poses, with an RMSD value below 2.0 Å indicating good agreement. Reasonable binding energy further supports the reliability of the docking protocol. Successful validation demonstrates that the docking method can reproduce the experimental binding mode, making it suitable for predicting the binding affinities and conformations of celecoxib derivatives in the context of structure-based drug design.

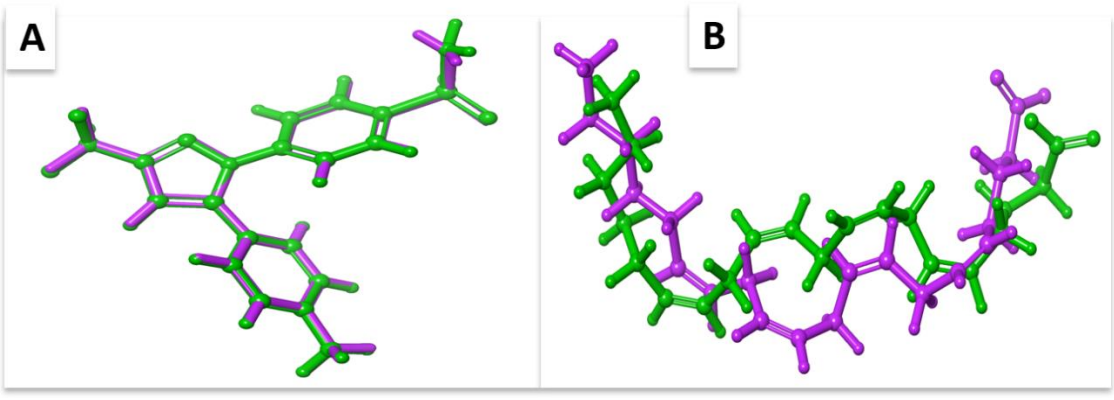

Figure 5.1. (A) Validation experiment showing re-docked and co-crystallized poses of celecoxib (PDB id 3LN1); **(B)** Validation poses of arachidonic acid (PDB id 3V99).

5.1.1.2. Docking Study into cyclooxygenase and lipoxygenase enzyme

All synthesized compounds were docked on COX-2 and 5-LOX (PDB id: 3LN1 and 3V99, respectively) enzyme targets using Schrödinger Maestro 2018.1 glide XP protocol. Firstly, grids were generated and validated by retrieving and re-docking the co-crystallized ligands (celecoxib and arachidonic acid) into COX and LOX protein targets. During validation RMSD value was calculated by superimposing the original co-crystallized ligand with the re-docked ligand pose, and its value was found to be 0.20 Å and 2.01 Å respectively against the COX and LOX targets. The outcomes of an *in vitro* and *in vivo* analysis revealed that compound **6k** was the most active compound from a series of synthesized compounds. The docking studies on the COX-2 enzyme revealed that compound **6k** binds efficiently to the key amino acid residues of the catalytic site like celecoxib. The biphenyl ring of compound **6k** showed hydrophobic interaction with Arg106, Ala513, Met508, Val335, Val509, Leu338, and Phe367 amino acid residues and enabled **6k** to occupy the COX-2 target's catalytic site. Additionally, it also displayed salt bridge interaction with Arg499 and Tyr371 amino acid. Furthermore, the oxygen atom of the oxadiazole ring in compound **6k** was also observed to establish a hydrogen bond interaction with His75 amino acid residue. The 4-F substituted phenyl ring extension showed hydrophobic interactions with Gln178, Phe504, and Ile503 amino acids (Figure 5.2). These outcomes were further supported by its favorable binding energy and conformational fit within the COX-2 ravine. Given its robust binding profile, compound **6k** emerges as a promising lead candidate, warranting further synthesis of analogues and comprehensive biological evaluation to investigate its therapeutic potential as a selective anti-inflammatory agent.

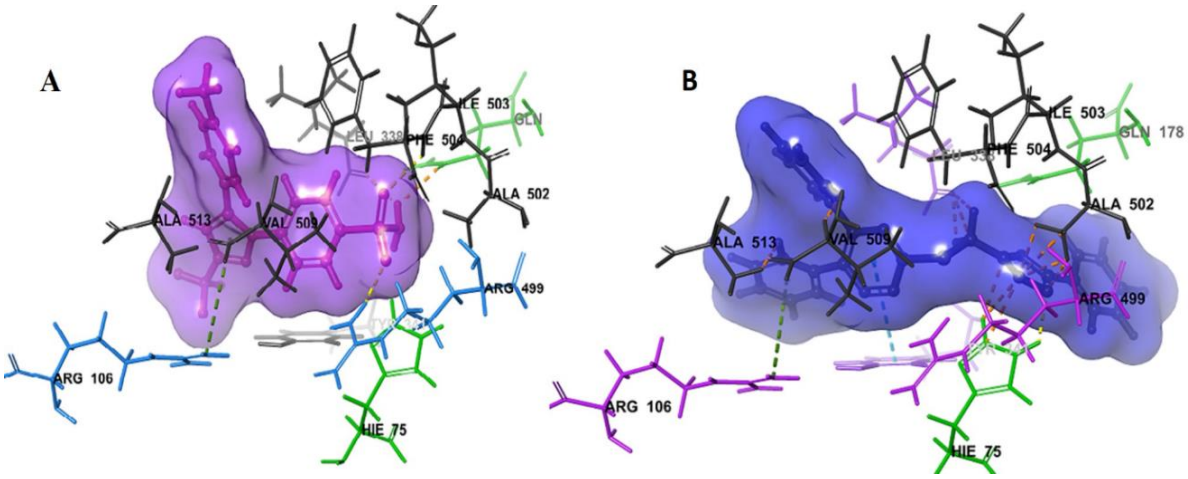

Figure 5.2. Docking pose of (A) Celecoxib and (B) compound 6k with COX-2 (PDB id: 3LN1)

The docking results on the 5-LOX manifested zileuton and compound **6k** interactions with the amino acid residues in the enzyme cleft. Both exhibited active hydrophobic interaction with His372, Asn180, Asn554, His367, and Phe555 amino acid residues critical for activity. Another important residue, Phe177, and Gln363 showed hydrogen bonding interaction with our designed compound **6k** (Figure 5.3). The 5-LOX catalytic site non-haem catalytic iron correlated by amino acids His367, His372, His550 and elongated pocket lined by Tyr181, Phe177, Ala603, and Ala410 (Manju, Ethiraj et al. 2018). Phe359, also an important residue responsible for the dual COX/LOX activity shows hydrophobic interaction with compound **6k**. The docking outcomes showed that the proposed chemical **6k** had a high binding affinity to the active site of the LOX enzyme, with favourable binding energies and critical interactions such as hydrogen bonding and hydrophobic contacts. These associations resemble or improve binding interactions found in the reference inhibitors, indicating that compound **6k** has the ability to inhibit LOX effectively. This underlines its potential as a lead compound for developing anti-inflammatory drugs that target the 5-LOX enzyme.

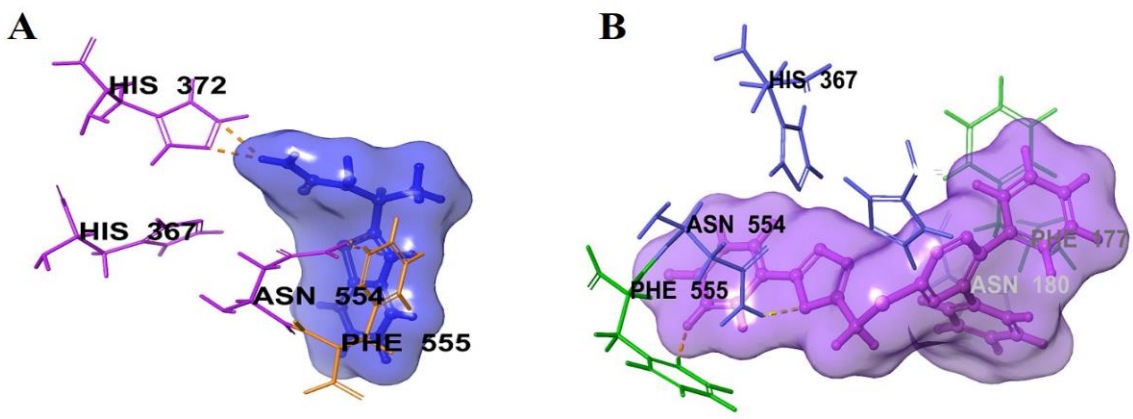

Figure 5.3. Docking pose of (**A**) Zileuton and (**B**) compound **6k** with 5-LOX (PDB id: 3V99)

5.1.1.3. Molecular dynamics

A molecular dynamics (MD) simulation experiments were carried out to observe the stability of the docked complex **6k** in both COX-2 and 5-LOX targets active site. The simulation runs were performed for 100 ns, and it is noteworthy that **6k** interacted with the amino acid residues of the COX-2 specific pocket as well as the 5-LOX enzyme catalytic cleft. The MD result of compound **6k** against COX-2 has shown almost perfect alignment after a 40 ns run and was stable up to 100 ns (Figure 5.4). The protein-ligand RMSD value of the simulated trajectory was also observed maximum of 2.7 Å and was in the acceptable limit of (1-3 Å). The designed derivative **6k** exhibited prominent hydrophobic interactions with Arg106 (50%), Leu335 (60%), Leu338 (35%), Val509 (30%), and Tyr341 (10%), confirming the designed compound stability in the COX-2 catalytic site. Hydrogen bonding interactions with His75 (10%), Ile503 (20%), and Phe504 (20%) along with hydrophobic interaction (20%) enable suitable binding interactions and might improve the inhibitory potential of the designed ligand. Molecular dynamics (MD) simulation investigations offer extensive insights into the dynamic functioning and stability of ligand-protein complexes as time progresses, that complement static docking studies. These computer simulations establish binding

interactions and evaluate conformation stability under physiologic environments, hence fostering trust in computational estimations.

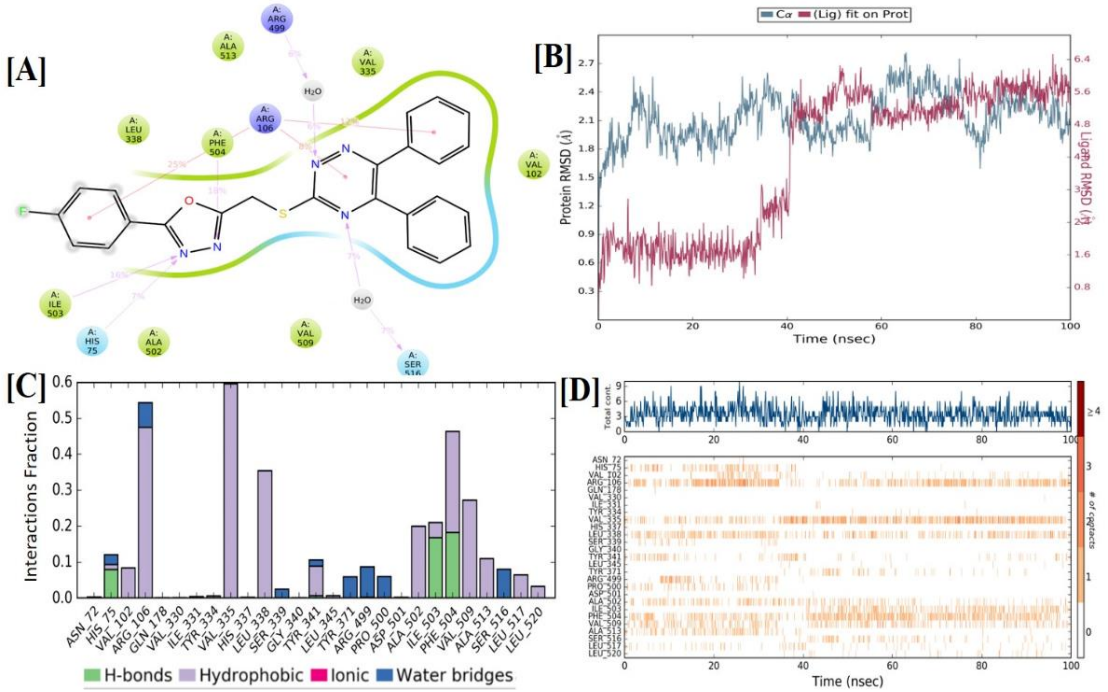

Figure 5.4. Molecular dynamic simulation study of the docked complex of **6k**-COX-2; [A] Graphical representation depicting percentage interactions; [B] RMSD graph of the compound for 100 ns run; [C] Histogram showing protein interaction with ligand **6k;** [D] A timeline representation of compound **6k**-COX-2.

The results of molecular dynamic simulation on the 5-LOX target convey that compound **6k** displayed stable protein-ligand alignment during the entire simulation run (Figure 5.5). The compound **6k** has shown strong hydrophobic interactions with critical amino acid residues His367 (50%), His 372 (25%), Leu607 (80%), Phe610 (60%), Ala410 (50%) (Rådmark, Werz et al. 2015). The docked complex has also shown a strong H-bond interaction with the residue Gln363 (60%) and water bridge mediated interaction (10%); also, Phe177 showed hydrophobic interaction (5%), along with water bridge mediated interaction (15%) which were accountable for overall protein-ligand complex stabilization.

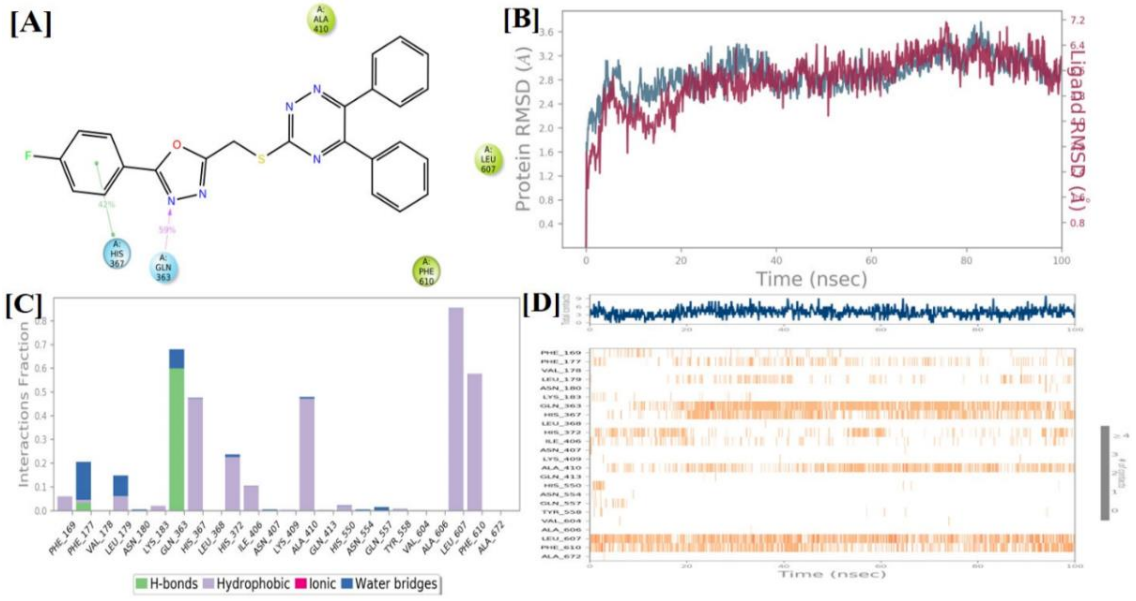

Figure 5.5. Molecular dynamic simulation study of the docked complex of **6k**-5-LOX; [A] Graphical representation depicting percentage interactions; [B] RMSD graph of compound for 100 ns run; [C] Histogram showing protein interaction with ligand **6k;** [D] A timeline representation of compound **6k**-5-LOX.

5.1.1.4.Drug-likeliness determination by Qikprop module

The drug-likeliness for the most potent derivative **6k** and the conventional drugs were calculated using the Qikprop Software module of Schrödinger Maestro 2018.1 as displayed in Table 5. 1. The prediction ensured that the compound abided by Lipinski's rule along with prediction of other important parameters including Log P estimation. The experimental Log P values in the range of ≤5 and other molecular properties predict if a novel compound with certain pharmacological potential would consider an orally active drug, vital in achieving a good bioavailability in humans (Shrivastava, Srivastava et al. 2017). By forecasting important ADMET characteristics, including permeability, solubility, and molecular descriptors, with predetermined standards for oral bioavailability, the QikProp module assesses drug-likeliness. Compounds that satisfy these requirements are deemed suitable for additional drug candidate development.

Table 5. 1. *In-silico* estimation of molecular properties

Compound	Mol wt.	Donor HB	Acceptor HB	QPlogPo/w	$n_{violations}$	QPlogPC16	QPlogPoct
Rule	< 500	≤ 5	≤ 10	≤ 5	≤ 1	4-18	8-43
6k	441.5	0.0	5.5	5.0	0	13.7	19.0
Celecoxib	381.4	2.0	5.5	3.3	0	10.8	20.2
Zileuton	236.3	3.0	3.7	0.9	0	8.5	14.4

Mol wt.; Molecular weight, Donor HB; Donor hydrogen bond, Acceptor HB; Acceptor hydrogen bond, QPlogPo/w; octanol-water partition coefficient, $n_{violations}$ = violations from Lipinski's rule, QPlogPC16; hexadecane/gas partition coefficient, QPlogPoct; octanol/gas partition coefficient.

5.1.2. Chemistry

5.1.2.1. Synthesis of novel compounds series I

The designed novel series of 5,6-diphenyl-1,2,4-triazine-3-thiol derivatives **6a-o** were synthesized and characterized. Intermediate compounds **2a-o** and **3a-o** were synthesized as per the procedures reported in previous work from our laboratory (Sharma, Tripathi et al. 2019). 5,6-diphenyl-1,2,4-triazine-3-thiol **(5)** was synthesized by treating benzil **(4)** with thiosemicarbazide in glacial acetic acid & water. The final compounds **(6a-o**) were obtained through nucleophilic substitution reaction on the -SH group **(**diphenyl-1,2,4-triazine-3-thiol) with that of the –Cl of the substituted 1,3,4-oxadiazole moiety. The progression and completion of each step were initially confirmed by TLC via different TLC visualizing reagents (Dragendorff's reagent, Bromocresol green, and iodine). The final structure of each compound was confirmed by ^{1}H and ^{13}C NMR spectroscopy, and also with high-resolution mass spectroscopy (HRMS). The % purity of the final compounds was also determined through high-performance liquid chromatography (HPLC).

The physicochemical characterization by state-of-the-art spectrometric methods have

illustrated that there was an absence of the characteristic signals of –NH-NH_2 of intermediates (**2a-o)** in 1,3,4-oxadiazole intermediates (**3a-o),** and the presence of methylene singlet with two protons at around of 4.94 ppm. The FT–IR spectrum of the compounds (**6a-o**) revealed a distinctive stretch band of aromatic -C–H stretching band at around 3000 to 2920 cm^{-1}, -C–O of an oxo at 1100-1175 cm^{-1}, and -C=N of a triazine at 1500-1685 cm^{-1}. The ^{1}H–NMR spectra of the derivatives **(6a-o)** have revealed the single peak of the methylene (–CH_2) at around 4.5-5.0 ppm. It seems to be a downfield shift that confirms the –CH_2 link to a heteroaromatic framework that supplies deshielding force. The diphenyl connected to the triazine ring is indicated by the aromatic region proton. The structural assignment is further supported by ^{13}C NMR spectroscopy. The 1,2,4-triazine nucleus appeared at 149.20-168.60 ppm in ^{13}C NMR spectra. The methylene carbon (–CH_2) peak was approximately around 22.68–24.68 ppm due to the influence of high electronegative sulphur. These spectroscopic data confirmed the formation of 5,6-diaryl-1,2,4-triazines-3-thiol compounds **(6a-o)**.

5.1.2.2. Characterization of synthesized derivatives

2-(((5,6-diphenyl-1,2,4-triazin-3-yl)thio)methyl)-5-(4-nitrophenyl)-1,3,4-oxadiazole (6a)

Light brown solid, yield 84%; mp 270-271 °C; TLC (Hexane/EtOAc 80:20 v/v); R_f = 0.56; FT-IR (υ cm^{-1}): 2920 (C–H), 1660 (C=N), 1331 (N=O); ^{1}H NMR (500 MHz, DMSO-d_6, ppm) δ 8.37 (d, *J* = 9.0 Hz, 2H), 8.14 (d, *J* = 9.0 Hz, 2H), 7.48 (d, *J* = 0.9 Hz, 1H), 7.47 (d, *J* = 1.3 Hz, 1H), 7.45 – 7.44 (m, 1H), 7.43 (dd, *J* = 4.4, 2.7 Hz, 2H), 7.41 (d, *J* = 1.3 Hz, 1H), 7.39 – 7.34 (m, 2H), 7.31 (t, *J* = 7.7 Hz, 2H), 4.98 (s, 2H); ^{13}C NMR (125 MHz, DMSO-d_6, ppm): δ_C 168.0, 165.1, 162.9, 155.7, 154.5, 149.1, 134.9, 134.7, 130.9, 129.7, 129.4, 129.2, 128.6, 128.4, 128.3, 127.8, 124.5, 24.0; HRMS $[M+1]^+$ Calculated 469.1077, Found 468.1085; HPLC purity: 95.54%, Retention time: 6.08 min.

2-(4-chlorophenyl)-5(((5,6-diphenyl-1,2,4-triazin-3-yl)thio)methyl)-1,3,4-oxadiazole (6b)

Yellow solid, yield 80%; mp 269-270 °C; TLC (Hexane/EtOAc 80:20 v/v); R_f = 0.58; FT-IR (υ cm^{-1}): 2982 (C–H), 1633 (C=N), 686 (—Cl); ^{1}H NMR (500 MHz, DMSO-d_6, ppm) δ 7.89 (d, *J* = 7.5 Hz, 2H), 7.63 (d, *J* = 7.9 Hz, 2H), 7.59 (d, *J* = 7.8 Hz, 1H), 7.62 (t, *J* = 7.9 Hz, 1H), 7.47 (d, *J* = 7.5 Hz, 2H), 7.45 (d, *J* = 8.2, Hz, 2H), 7.38 (d, *J* = 7.4 Hz, 2H), 7.33 (t, *J* = 7.4 Hz, 2H), 4.96 (s, 2H); ^{13}C NMR (125 MHz, DMSO-d_6, ppm): δ_C 168.6, 164.8, 164.0, 156.2, 155.0, 137.2, 135.5, 135.2, 131.4, 130.2, 130.0, 129.8, 129.7, 128.9, 128.8, 128.6, 122.5, 24.4; HRMS $[M+1]^+$ Calculated 458.0836, Found 458.0829; HPLC purity: 99.96%, Retention time: 4.1 min.

2-(3-chlorophenyl)-5-(((5,6-diphenyl-1,2,4-triazin-3-yl)thio)methyl)-1,3,4-oxadiazole (6c)

Brown solid, yield 77%; mp 252-254 °C; TLC (Hexane/EtOAc 80:20 v/v); R_f = 0.57; FT-IR (υ cm^{-1}): 2979 (C–H), 1627 (C=N), 763 (—Cl); ^{1}H NMR (500 MHz, DMSO-d_6, ppm) δ 7.89 (s, 1H), 7.86 (d, *J* = 7.7 Hz, 1H), 7.68 (d, *J* = 7.9 Hz, 1H), 7.60 (t, *J* = 7.9 Hz, 1H), 7.48 (d, *J* = 7.5 Hz, 2H), 7.44 (dd, *J* = 9.3, 7.9 Hz, 4H), 7.39 (d, *J* = 7.4 Hz, 2H), 7.31 (t, *J* = 7.6 Hz, 2H), 4.95 (s, 2H); ^{13}C NMR (125 MHz, DMSO-d_6, ppm): δ_C 164.6, 163.1, 162.3, 155.7, 135.0, 134.7, 134.0, 131.9, 131.5, 130.9, 129.7, 129.4, 129.3, 128.5, 128.3, 125.9, 125.1, 23.9; HRMS $[M+1]^+$ Calculated 458.0836, Found 458.0834; HPLC purity: 95.04%, Retention time: 5.66 min.

2-(((5,6-diphenyl-1,2,4-triazin-3-yl)thio)methyl)-5-(3-methoxyphenyl)-1,3,4-oxadiazole (6d)

Yellow solid, yield 75%; mp 259-260 °C; TLC (Hexane/EtOAc 80:20 v/v); R_f = 0.57; FT-IR (υ cm^{-1}): 2934 (C–H), 1674 (C=N), 1102 (C—O); ^{1}H NMR (500 MHz, DMSO-

d_6, ppm): δ 7.72 – 7.55 (m, 4H), 7.49 – 7.33 (m, 7H), 7.24 (d, *J* = 15.6 Hz, 2H), 7.12 (s, 1H), 4.96 (s, 2H), 3.80 – 3.72 (m, 3H); ^{13}C NMR (125 MHz, DMSO-d6,ppm): δ_C 168.6, 164.6, 160.0, 156.2, 155.0, 135.4, 135.1, 131.4, 131.2, 130.2, 129.9, 129.7, 128.9, 128.8, 124.7, 119.1, 118.5, 111.6, 55.8, 24.4; HRMS $[M+1]^+$ Calculated 454.1332, Found 454.1349; HPLC purity: 99.94%, Retention time: 4.6 min.

2-(((5,6-diphenyl-1,2,4-triazin-3-yl)thio)methyl)-5-phenyl-1,3,4-oxadiazole (6e)

Dark brown solid, yield 78%; mp 251-253 °C; TLC (Hexane/EtOAc 80:20 v/v); R_f = 0.59; FT-IR (υ cm^{-1}): 2988 (C–H), 1659 (C=N), 1558 (C—H); ^{1}H NMR (500 MHz, DMSO-d_6, ppm) δ 7.93 – 7.89 (m, 4H), 7.61– 7.52 (m, 2H), 7.43 – 7.31 (m, 9H), 4.94 (s, 2H); ^{13}C NMR (125 MHz, DMSO-d_6, ppm): δ_C 168.6, 164.7, 164.6, 156.2, 155.0, 135.5, 135.2, 132.5, 131.4, 130.2, 130.0, 129.9, 129.7, 128.9, 128.9, 127.1, 126.8, 123.6, 24.4; HRMS $[M+1]^+$ Calculated 424.1226, Found 424.1211; HPLC purity: 99.98%, Retention time: 5.5 min

2-(2,4-dichlorophenyl)-5-(((5,6-diphenyl-1,2,4-triazin-3-yl)thio)methyl)-1,3,4-oxadiazole (6f)

Brown solid, yield 75%; mp 271-272 °C; TLC (Hexane/EtOAc 80:20 v/v); R_f = 0.56; FT-IR (υ cm^{-1}): 2992 (C–H), 1627 (C=N), 763 (C—Cl); ^{1}H NMR (500 MHz, DMSO-d_6, ppm): δ 7.88 (d, *J* = 7.6 Hz, 1H), 7.61 (d, *J* = 7.7 Hz, 1H), 7.49 – 7.40 (m, 9H), 7.31 (t, *J* = 13.3 Hz, 2H), 4.99 (s, 2H); ^{13}C NMR (125 MHz, DMSO-d_6 ppm): δ_C 168.5, 165.1, 162.2, 156.1, 155.0, 137.6, 135.4, 135.1, 133.2, 133.0, 132.7, 131.4, 131.2, 130.2, 129.9, 129.7, 128.9, 128.8, 128.6, 121.8, 24.3; HRMS $[M+1]^+$ Calculated 492.0447, Found 492.0431; HPLC purity: 96.92%, Retention time: 4.2 min

2-(((5,6-diphenyl-1,2,4-triazin-3-yl)thio)methyl)-5-(4-(trifluoromethoxy) phenyl)-1,3,4-oxadiazole (6g)

Dark brown solid, yield 85%; mp 262-264 °C; TLC (Hexane/EtOAc 80:20 v/v); R_f = 0.58; FT-IR (υ cm^{-1}): 2977 (C–H), 1687 (C=N), 1192 (C—F); ^{1}H NMR (500 MHz, DMSO-d_6, ppm): δ 7.67–7.63 (m, 2H), 7.61-7.49 (m, 10H), 7.41-7.39 (m, 2H), 4.96 (s, 2H); ^{13}C NMR (125 MHz, DMSO-d_6, ppm): δ_C 163.6, 162.2, 156.7, 155.1, 153.8, 152.8, 134.8, 133.0, 131.8, 131.6, 131.6, 129.7, 129.7, 129.4, 128.5, 127.6, 124.1, 121.8, 121.6, 120.7, 23.6; HRMS $[M+1]^+$ Calculated 508.1049, Found 508.1018; HPLC purity: 99.95%, Retention time: 5.9 min

2-(((5,6-diphenyl-1,2,4-triazin-3-yl)thio)methyl)-5-(2,4,5-trifluorophenyl)-1,3,4-oxadiazole (6h)

Dark brown solid, yield 80%; mp 274-276 °C; TLC (Hexane/EtOAc 80:20 v/v); R_f = 0.54; FT-IR (υ cm^{-1}): 2928 (C–H), 1606 (C=N), 1088 (C—F); ^{1}H NMR (500 MHz, DMSO-d_6, ppm) δ 7.98 (dd, *J* = 15.9, 9.0 Hz, 1H), 7.86 (dd, *J* = 16.7, 10.2 Hz, 1H), 7.48 (d, *J* = 7.5 Hz, 2H), 7.43 (dd, *J* = 11.6, 7.1 Hz, 4H), 7.40 – 7.36 (m, 2H), 7.31 (t, *J* = 7.5 Hz, 2H), 4.97 (s, 2H); ^{13}C NMR (125 MHz, DMSO-d_6, ppm): δ_C 168.5, 165.1, 156.1, 154.9, 135.4, 135.4, 135.1, 131.3, 130.1, 129.8, 129.7, 128.7, 117.8, 117.6, 108.7, 108.5, 108.5, 108.3, 24.3. HRMS $[M+1]^+$ Calculated 478.0943, Found 478.0949; HPLC purity: 98.32%, Retention time: 5.53 min

2-(((5,6-diphenyl-1,2,4-triazin-3-yl)thio)methyl)-5-(4-methoxyphenyl)-1,3,4-oxadiazole (6i)

Brown solid, yield 86%; mp 260-262 °C; TLC (Hexane/EtOAc 80:20 v/v); R_f = 0.59; FT-IR (υ cm^{-1}): 2993 (C–H), 1653 (C=N), 1087 (O—C); ^{1}H NMR (500 MHz, DMSO-d_6, ppm): δ 7.84 – 7.83 (m, 2H), 7.50 – 7.49 (m, 2H), 7.46 – 7.31 (m, 8H), 7.10 (d, *J* =

14.6 Hz, 2H), 4.93 (s, 2H), 3.82 – 3.78 (m, 3H); ^{13}C NMR (125 MHz, DMSO-d_6,ppm): δ_C 168.6, 164.6, 163.9, 162.7, 162.4, 156.1, 154.9, 135.5, 135.2, 131.4, 130.3, 130.2, 139.8, 129.7, 128.9, 128.8, 128.7, 115.9, 115.4, 115.3, 114.4, 55.9, 24.4; HRMS $[M+1]^+$ Calculated 441.1254, Found 441.1239; HPLC purity: 94.90%, Retention time: 4.1 min.

2-(4-chloro-3-nitrophenyl)-5-(((5,6-diphenyl-1,2,4-triazin-3-yl)thio) methyl)-1,3,4-oxadiazole (6j)

Brown solid, yield 75%; mp 251-252 °C; TLC (Hexane/EtOAc 80:20 v/v); R_f = 0.57; FT-IR (υ cm^{-1}): 2922 (C–H), 1649 (C=N), 689 (C—Cl), 1324 (N=O); ^{1}H NMR (500 MHz, DMSO-d_6, ppm): δ 7.91 (s, 1H), 7.79 (s, 1H), 7.66 (s, 1H), 7.62 – 7.49 (m, 4H), 7.46 – 7.44 (m, 4H), 7.33 (d, *J* = 8.5 Hz, 2H), 4.86 (m, 2H); ^{13}C NMR (125 MHz, DMSO-d_6, ppm): δ_C 168.6, 167.2, 156.7, 155.1, 152.8, 148.5, 134.8, 133.0, 132.5, 131.6, 131.1, 129.7, 129.6, 129.4, 128.5, 127.6, 124.0, 123.4, 23.6; HRMS $[M+1]^+$ Calculated 503.0687, Found 503.0671; HPLC purity: 95.70%, Retention time: 5.1 min.

2-(((5,6-diphenyl-1,2,4-triazin-3-yl)thio)methyl)-5-(4-fluorophenyl)-1,3,4-oxadiazole (6k)

Brown solid, yield 72%; mp 268-270 °C; TLC (Hexane/EtOAc 80:20 v/v); R_f = 0.61; FT-IR (υ cm^{-1}): 2982 (C–H), 1587 (C=N), 1082 (C—F); ^{1}H NMR (500 MHz, DMSO-d_6, ppm) δ 7.96 (dd, *J* = 8.8, 5.3 Hz, 2H), 7.49 (d, *J* = 7.3 Hz, 2H), 7.45 (dd, *J* = 4.5, 2.3 Hz, 4H), 7.42 (d, *J* = 3.9 Hz, 2H), 7.40 (d, *J* = 2.1 Hz, 2H), 7.33 (d, *J* = 7.6 Hz, 2H), 4.95 (s, 2H); ^{13}C NMR (125 MHz, DMSO-d_6, ppm): δ_C 164.6, 163.1, 162.3, 155.7, 135.0, 134.7, 134.0, 131.9, 130.9, 129.7, 129.4, 129.3, 128.5, 128.3, 125.9, 125.1, 23.9; HRMS $[M+1]^+$ Calculated 442.1132, Found 442.1119; HPLC purity: 98.42%, Retention time: 5.58 min.

2-(((5,6-diphenyl-1,2,4-triazin-3-yl)thio)methyl)-5-(2-nitrophenyl)-1,3,4-oxadiazole (6l)

Brown solid, yield 79%; mp 268-270 °C; TLC (Hexane/EtOAc 80:20 v/v); R_f = 0.54; FT-IR (υ cm^{-1}): 2954 (C–H), 1660 (C=N), 1331 (N=O); ^{1}H NMR (500 MHz, DMSO-d_6, ppm) δ 8.02 (d, *J* = 9.0 Hz, 1H), 7.89 (d, *J* = 7.0 Hz, 2H), 7.84 (d, *J* = 2.1 Hz, 2H), 7.82 (d, *J* = 1.4 Hz, 1H), 7.81 – 7.79 (m, 1H), 7.59 (dd, *J* = 4.1, 2.4 Hz, 2H), 7.43 (d, *J* = 1.3 Hz, 1H), 7.37 – 7.33 (m, 2H), 7.31 (t, *J* = 7.6 Hz, 2H), 4.98 (s, 2H); ^{13}C NMR (125 MHz, DMSO-d_6, ppm): δ_C 163.6, 156.7, 155.1, 152.8, 152.8, 148.2, 134.8, 133.9, 133.0, 132.3, 131.6, 129.7, 129.4, 128.5, 127.6, 126.6, 126.1, 124.0, 24.6; HRMS $[M+1]^+$ Calculated 469.1077, Found 469.1059. HPLC purity: 97.89%, Retention time: 5.61 min.

2-(3,5-dinitrophenyl)-5-(((5,6-diphenyl-1,2,4-triazin-3-yl)thio)methyl)-1,3,4-oxadiazole (6m)

Light brown solid; yield 82%; mp 260-262 °C; TLC (Hexane/EtOAc 80:20 v/v); R_f = 0.64; FT-IR (υ cm^{-1}): 2926 (C–H), 1651 (C=N), 1334 (N=O); ^{1}H NMR (500 MHz, DMSO-d_6, ppm): δ 9.22 (s, 1H), 8.93 – 8.91 (m, 2H), 8.61 – 7.56 (m, 3H), 7.52 – 7.49 (m, 1H), 7.45 – 7.38 (m, 4H), 7.31 (d, *J* = 14.2 Hz, 2H), 4.81 (s, 2H); δ_C 163.6, 161.1, 156.7, 155.1, 152.8, 147.4, 134.8, 133.0, 131.6, 129.7, 129.7, 129.4, 128.5, 127.9, 127.6, 127.3, 119.5, 22.6; HRMS $[M+1]^+$ Calculated 514.0928, Found 514.0941. HPLC purity: 99.14%, Retention time: 5.74 min.

4-(5-(((5,6-diphenyl-1,2,4-triazin-3-yl)thio)methyl)-1,3,4-oxadiazol-2-yl) benzonitrile (6n)

Light brown solid, yield 85%; mp 262-263 °C; TLC (Hexane/EtOAc 80:20 v/v); R_f = 0.58; FT-IR (υ cm^{-1}): 2927 (C–H), 1661 (C=N), 2228 (C≡N); ^{1}H NMR (500 MHz, DMSO-d_6, ppm) δ 8.29 (s, 1H), 8.19 (d, *J* = 7.7 Hz, 1H), 8.08 (d, *J* = 7.7 Hz, 1H), 7.77 (t, *J* = 7.9 Hz, 1H), 7.49 (d, *J* = 7.3 Hz, 2H), 7.46 – 7.41 (m, 4H), 7.39 (d, *J* = 7.4 Hz, 2H), 7.31 (t, *J* = 7.7 Hz, 2H), 4.96 (s, 2H); ^{13}C NMR (125 MHz, DMSO-d_6, ppm): δ_C 168.1,

164.8, 162.8, 155.7, 154.5, 135.4, 135.0, 130.9, 130.8, 130.8, 129.9, 129.7, 129.4, 129.2, 128.4, 128.3, 127.6, 112.6, 23.9; HRMS $[M+1]^+$ Calculated 449.1179, Found 449.1191; HPLC purity: 97.16%, Retention time: 4.64 min.

3-(5-(((5,6-diphenyl-1,2,4-triazin-3-yl)thio)methyl)-1,3,4-oxadiazol-2-yl) benzonitrile (6o)

Brown solid, yield 71%; mp 255-256 °C; TLC (Hexane/EtOAc 80:20 v/v); R_f = 0.59; FT-IR (υ cm^{-1}): 2925 (C–H), 1663 (C=N), 2231 (C≡N); ^{1}H NMR (500 MHz, DMSO-d_6, ppm) δ 8.31 (d, *J* = 7.1 Hz, 2H), 8.15 (d, *J* = 7.9 Hz, 2H), 7.79 (d, *J* = 7.5 Hz, 2H), 7.54 – 7.39 (m, 4H), 7.36 (d, *J* = 7.4 Hz, 2H), 7.31 (t, *J* = 7.6 Hz, 2H), 4.98 (s, 2H); ^{13}C NMR (125 MHz, DMSO-d_6, ppm): δ_C 168.5, 165.2, 163.3, 156.2, 155.0, 136.2, 135.8, 135.4, 131.6, 131.3, 131.3, 130.6, 130.3, 129.8, 129.7, 128.9, 124.8, 118.1, 113.1, 113.1, 24.4; HRMS $[M+1]^+$ Calculated 449.1179, Found 449.1193. HPLC purity: 97.16%, Retention time: 4.64 min.

5.1.3. Biological screening

5.1.3.1.In Vitro Biological Evaluation

5.1.3.1.1. *In vitro* assay for COX-1 and COX-2 inhibitory activity

The inhibitory strength of compounds **(6a-o)** was investigated by employing the colorimetric inhibition assay, and the IC_{50} values were calculated (Table 5.2). The tested derivatives effectively suppressed COX-2 over COX-1; (IC_{50} values range from 0.33 to 4.43 µM for COX-2 and 21.49 to 45.98 µM for COX-1, respectively). The novel triazine hybrids **6a, 6c, 6h, 6k,** and **6o** exhibited potent COX-2 inhibitory profiles comparable to standard celecoxib (IC_{50} = 1.81 ± 0.13 µM). Notably, the COX-2 inhibitory activity of novel hybrids **6c (**IC_{50} = 0.84 ± 0.03 µM) and **6k (**IC_{50} = 0.33 ± 0.02 µM) surpass celecoxib activity. The phenyl group substituted with an electron-donating group like -

OCH_3 showed moderate inhibitory potential, while electron-withdrawing groups (-NO_2, -CN, -Cl, and -F) have shown increased inhibitory activity. In terms of COX-2 inhibition selectivity, all the hybrids have examined substantial COX-2 inhibition over COX-1.

Table 5.2. Results of COX-1/COX-2 and 5-LOX enzyme inhibition assay

Comp.	-R	IC_{50} COX-2 (μM)[a]	IC_{50} COX-1 (μM)[a]	COX-2 Selectivity Index[b]	IC_{50} 5-LOX (μM)[a]
6a	4-NO_2	1.88 ± 0.06	36.16 ± 0.44	19.24	10.90 ± 0.20
6b	4-Cl	2.19 ± 0.08	41.46 ± 0.68	18.95	9.18 ± 0.30
6c	3-Cl	**0.84 ± 0.03**	37.95 ± 0.57	45.16	**8.75 ± 0.09**
6d	3-OCH_3	3.56 ± 0.10	44.17 ± 0.04	12.40	12.98 ± 0.53
6e	Ph	3.31 ± 0.07	45.98 ± 0.12	13.91	13.76 ± 0.85
6f	2,4-diCl	3.04 ± 0.10	32.75 ± 0.27	10.79	11.45 ± 0.32
6g	3-OCF_3	2.27 ± 0.04	44.86 ± 0.38	19.76	19.76 ± 0.11
6h	2,4,5-triF	1.63 ± 0.14	21.49 ± 0.82	13.19	9.27 ± 0.21
6i	4-OCH_3	3.83 ± 0.01	40.09 ± 0.08	10.46	11.19 ± 0.46
6j	4-Cl-3-NO_2	4.43 ± 0.10	41.25 ± 0.69	9.32	16.16 ± 0.80
6k	4-F	**0.33 ± 0.02**	25.79 ± 0.24	77.40	**4.90 ± 0.22**
6l	2-NO_2	2.07 ± 0.10	41.29 ± 0.36	19.94	9.91 ± 0.31
6m	3,5-diNO_2	2.53 ± 0.12	42.64 ± 0.04	16.83	12.75 ± 0.11
6n	4-CN	1.40 ± 0.08	34.65 ± 0.05	24.81	10.19 ± 0.34
6o	3-CN	2.65 ± 0.06	23.53 ± 0.97	8.87	9.97 ± 0.33
Celecoxib	-	1.81 ± 0.13	39.70 ± 0.01	28.59	Nd
Zileuton	-	nd	nd	nd	15.04 ± 0.18
Indomethacin	-	3.72 ± 0.04	3.77 ± 0.01	1.01	Nd

[a]All values are reported in mean ± SD.

[b] Selectivity index for COX-2 = IC_{50} of COX-1/IC_{50} of COX-2

[nd] Not determined

5.1.3.1.2. *In vitro* 5-LOX inhibition assay

The *in vitro* Lipoxygenase inhibitory activity of compounds **6a-o** was assessed and calculated. The results indicated that the majority of the tested derivatives were effective 5-LOX enzyme inhibitors outperforming zileuton (Table 5.2). The tested compounds **6c** (IC_{50} = 8.75 ± 0.09 µM) and **6k** (IC_{50} = 4.90 ± 0.22 µM) demonstrated superior LOX inhibitory activities than standard zileuton (IC_{50} = 15.04 ± 0.18 µM). The substitution of phenyl group with 4-F derivative elicits an excellent ability to inhibit 5-LOX activity; thus, it was selected for further *in vivo* experiments and *in silico* trials to confirm the dual COX-2 and 5-LOX inhibition potentials.

5.1.3.1.3. Structure Activity Relationship (SAR)

The *in vitro* COX-2 and 5-LOX inhibitory activity, as described in Table 5.2, suggested that the electronic distribution around substituted phenyl ring attached to oxadiazole moiety in the designed series of compounds has moderate to excellent activity in comparison with standard celecoxib and zileuton. The presence of EWG (-NO_2) at the C-2 position of the phenyl ring attached to oxadiazole showed moderate COX-2 and 5-LOX activity. The substitution of EWG (-CN and -OCF_3) at the C-3 position of the phenyl ring also showed moderate COX-2 and 5-LOX inhibition while increased inhibitory activity was observed with the -Cl group at the same position. Disubstitution of EWG at 2, 4 (di-Cl)), and 3, 5 (di -NO_2) positions on phenyl ring have also shown moderate inhibitory activity against both the targets. The EWG at 2, 4, and 5-position of phenyl ring (tri-F) has shown increased inhibitory activity compared to celecoxib and zileuton. The substitutions at the C-4 position with -Cl, -NO_2, -CN, -F have also shown increased

inhibitory activity of compounds. Compound **6k** bearing 4-F substitution on the phenyl ring has shown the maximum inhibitory potential against both COX-2 and 5-LOX enzymes. The presence of EDG at C-3 and C-4 positions (-OCH_3) resulted in moderate inhibitory activity. In our previous work, the substitution of chloromethyl oxadiazole derivative at the 2-N position of 1,2,4-triazin-3(2H)-one has resulted in favorable selective COX-2 inhibitory activity while the present work reflects that the substitution of chloromethyl oxadiazole derivative at thiol group of 1, 2, 4-triazine ring resulted in better inhibitory activity against both COX-2 and 5-LOX.

5.1.3.2.Pharmacological Evaluation

5.1.3.2.1. Acute oral toxicity studies

The acute toxicity investigation has been carried out in accordance with OECD 423 recommendations to examine the safety profile of compounds **6c** and **6k** before exposing rats to *in vivo* models. The results indicated no toxic or aberrant behaviors in the animals; the compounds tolerance remained fair up to a dose of 500 mg/kg. Moreover, there was no mortality despite the highest dose of 500 mg/kg body weight for 14 days following oral administration of the compounds, showing a considerable safety margin. Animals have been sacrificed for histological investigation of the kidney, liver, stomach, and lungs, which revealed no significant variations as compared to controls.

5.1.3.2.2. Carrageenan-induced paw edema

Carrageenan-induced rat paw edema is a well-explored experimental model for evaluating acute inflammatory response. The paw edema is biphasic at an early stage containing histamine, kinins & serotonin pro-inflammatory agents accompanied by the latter stage release of prostaglandins (Vinegar, Schreiber et al. 1969, Marzouk, Marzouk et al. 2010). The anti-inflammatory property of the identified derivatives **6c** and **6k** in carrageenan-induced rat paw edema was evaluated. The carrageenan triggers a significant

inflammatory response, such that it can be detected in 30 minutes once delivered locally in the rat paw sub-plantar region. Mean variations in paw edema thickness enable recording percentage inhibition of edema as determined for one-hour intervals up to six hours from induction of inflammation (Table 5.3). The study findings indicated significant inhibitory potency of synthesized derivatives comparable with standard drug indomethacin (Indo).

The anti-inflammatory impact for synthesized derivatives occurred until 5 h, for which duration was expected to attain maximal intensity, accompanied by a marked decrease. The maximum percentage protection against paw edema caused by carrageenan for indomethacin (62.71%) was observed at 4 h, followed by a marked decrease. Selected compounds **6c (**58.09%**)** and **6k (**58.34%**)** recorded maximum percentage protection against carrageenan-induced paw edema at 5 h.

Selected derivatives displayed consistent behaviour with indomethacin, enabling further assessment. The significant activity of the compound was observed in mitigating inflammation in the late phase attributable to the compounds' potential to suppress prostaglandins mediator activation.

Table 5. 3. Carrageenan-Induced Paw edema

	Swelling thickness in mm (% inhibition)						
	0 h	**1 h**	**2h**	**3 h**	**4 h**	**5 h**	**6 h**
Control	3.57 ± 0.20	8.54 ± 0.21	8.72 ± 0.43	8.61 ± 0.26	8.54 ± 0.20	8.36 ± 0.23	8.18 ± 0.16
Indo 10	3.62 ± 0.24	3.65 ± 0.21[a] (57.2)	3.56 ± 0.21[a] (59.2)	3.40 ±0.17[a] (60.53)	3.18 ± 0.09[a] (62.71)	3.15 ±0.24[a] (62.27)	3.13 ± 0.05[a] (61.78)
6c	3.59 ± 0.20	5.56 ± 0.77[a,b] (34.88)	4.75 ± 0.57[a,b] (45.49)	4.42 ± 0.35[a,b] (48.64)	3.99 ± 0.41[a] (53.24)	3.50 ± 0.34[a] (58.09)	3.52 ± 0.32[a] (56.94)
6k	3.63 ± 0.28	5.66 ± 0.50[a,b] (33.72)	5.09 ± 0.41[a,b] (41.67)	4.54 ± 0.46[a,b] (47.31)	4.13 ± 0.48[a,b] (51.68)	3.48 ± 0.34[a] (58.34)	3.51 ± 0.34[a] (57.05)

Data presented in the mean ± SD; Control: 0.3 % Na CMC solution (10 ml/kg/p.o.) in distilled water; Indo 10 (Indomethacin, 10 mg/kg, p.o.) in 0.3 % Na CMC was employed as the standard

group; The investigated derivatives were administered orally at an equimolar dosage of 10 mg/kg indomethacin in a 0.3 % w/v Na CMC solution; "Edema inhibition (%) of the tested compounds 6c and 6k relative to edema inhibition (%) of the standard drug demonstrated mean protection (%) at 6 h". [a]$p < 0.05$ = Control; [b]$p < 0.05$ = Indo 10.

5.1.3.2.3. Arachidonic acid-induced paw edema

The experimental model in which arachidonic acid is used to induce paw edema in rats distinguishes COX from LOX. Unlike COX inhibition, this model is especially responsive to LOX suppression (DiMartino, Campbell et al. 1987, Shrivastava, Srivastava et al. 2017). After 30 minutes of sub-plantar arachidonic acid injection, it showed substantial swelling, or even in 60 minutes hits a peak. The exploratory compounds were administered orally, arachidonic acid-mediated paw edema was significantly reduced, and the compounds seem to be impervious to COX inhibition. Studies indicated that besides the selective LOX inhibitor zileuton with 71.38% protection against inflammation, the test compound **6c**, containing a 3–chlorophenyl group on oxadiazole substituents, manifested remarkably similar 68.07% protection. Also, compound **6k** exhibited 62.48% protection against arachidonic acid-induced edema (Table 5. 4). Thus, the selected derivatives demonstrated to exert an anti-inflammatory effect by curtailing the LOX mechanism.

Table 5. 4. Arachidonic Acid-Induced paw edema

Compound	**Swelling thickness (mm)** (Mean ± S.D)	% protection
Control	6.70 ± 0.28	-
Zileuton	1.92 ± 0.11	71.38
6c	2.14 ± 0.18	68.07
6k	2.16 ± 0.14	62.48

"Standard group consisted of Zileuton (10 mg/kg/per oral) in 0.3% w/v carboxymethyl cellulose sodium"

5.1.3.2.4. Gastric ulcerogenic liabilities

❖ ***Gross evaluation***

The ulcerogenic potential of compounds **6c** and **6k** was further examined and assessed utilizing ulcer indices and ulcerative percentages, as shown in Table 5.5. Macroscopic and microscopic examinations revealed that the stomachs of the control group rats were completely free of ulcers. In contrast, rats given indomethacin developed aggressive ulcers and perforation throughout their stomachs, with ulcer scores with mean, standard deviations of 3.16 ± 0.26 (ulcer index 316.66). Indomethacin treated group showed nuclei aggregation and disruption of cellular structure when observed at higher magnification, whereas the tested derivatives showed intact cellular structure. In comparison to the control and indomethacin, compound **6c** caused mild mucosal injuries in the stomachs of some rats. Conversely, the compound **6k**-treated group (ulcer index 4.37) exhibited insignificant levels of lesions or mucosal injuries in their stomach. These observations confirm the compounds' excellent gastrointestinal tolerance compared to indomethacin, as evidenced by reduced ulcerogenic potential and better safety profiles in preclinical studies. This suggests their potential for safer therapeutic applications in managing inflammatory conditions (Figure 5.6).

Table 5.5. Evaluation of the gross ulcerogenic effect of celecoxib, Indomethacin, **6c**, and **6k**

Compound Code	Ulceration (%)	Ulcer Score	Ulcer Index
Control	0	0	0
Indomethacin	100	$3.16 \pm 0.26^{*}$	316.66
6c	10	$0.16 \pm 0.07^{*\#}$	16.66
6k	2.83	$0.04 \pm 0.01^{\#@}$	4.37

The mean ± SD used to present the data; Control: 0.3 % Na CMC solution (10 ml/kg/p.o.) in distilled water; Indomethacin (10 mg/kg, p.o.) in 0.3 % Na CMC was employed as the standard

group; Test compounds were given at an equimolar dose of 10mg/kg indomethacin; *p < 0.05 Control, #p < 0.05 Indomethacin, @p < 0.05 6c.

❖ ***Microscopic evaluation***

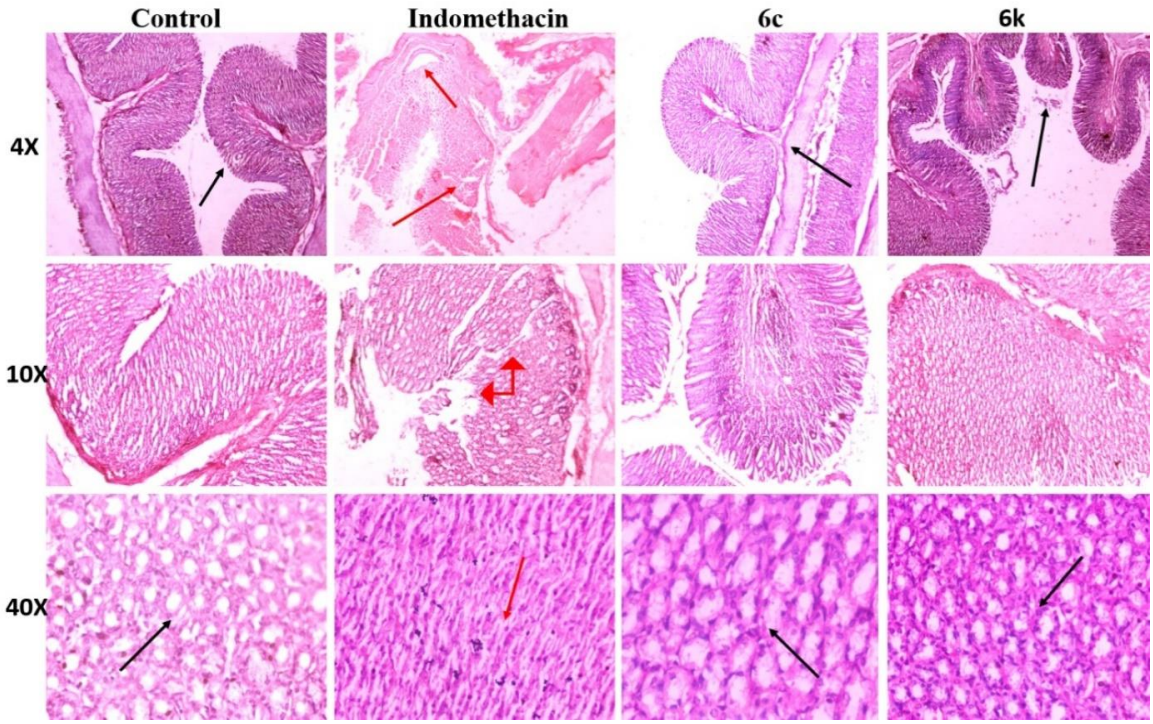

Figure 5.6. Histology photomicrographs (4X; 10X; 40X, shown vertically) *: Control revealed the normal adjoining gastric mucosal framework protruding into gastric pits (black arrow); Gastric mucosa of indomethacin treated rats* (red arrows) showing exuviating surface epithelium due to ulceration; Compound **6c** and Compound **6k** treated rat groups* showed little or no indication of ulceration, (black arrow) showing normal mucosal framework.

5.1.3.2.5. Biochemical Analysis

Reactive oxygen species (ROS) are known to exacerbate inflammation. Antioxidants interfere with the production and inhibition of ROS (Fomenko, Bondarchuk et al. 2015). Major free radical scavengers and antioxidants also aid in anti-inflammatory therapies. Glutathione (GSH) level, and lipid peroxide (LPO) actions, have been analyzed in an attempt to examine the possible role of oxidative stress triggered gastric mucosal damage and the results are presented in Figure 5.7. In our study, indomethacin exerted aggressive oxidative stress on the stomach (gastric tissue) which showed a highly

significant difference compared to control groups, which might be a preliminary cause of ulcers. Compounds **6c** and **6k** both are showing highly significant effects by increasing the antioxidant activity compared to celecoxib, zileuton and indomethacin groups.

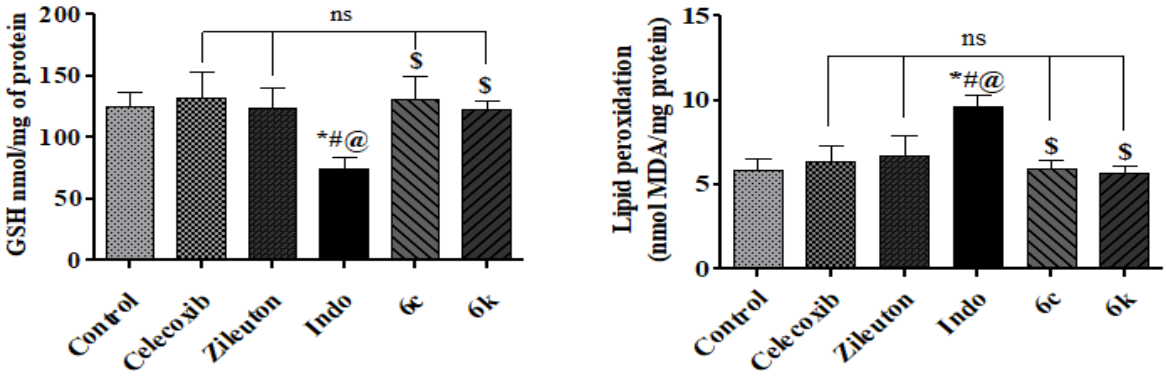

Figure 5.7. All values reported as mean ± standard deviation; rats (n = 6)/group; *p < 0.05 vs. Control (0.3 % sodium CMC mixture in distilled water; 10ml/kg given orally); #p < 0.05 vs. Celecoxib (10 mg/kg given orally) in 0.3 % sodium CMC solution; @ p < 0.05 vs. Zileuton (10 mg/kg given orally); $ p < 0.05 vs. Indomethacin (10 mg/kg given orally) in 0.3 % sodium CMC solution; ¥ p < 0.05 vs. **6c** (10 mg/kg given orally); (Repeated measure one-way ANOVA followed by Tukey's test).

5.1.3.2.6. Evaluation of cardiotoxic effect:

Selected compounds **6c** and **6k** were further evaluated for cardiotoxic liability in rats. Myocardial infarction was diagnosed using cardiac biomarkers such as creatine kinase-MB (CK-MB) and cardiac troponin I (cTn-I). The use of cardiac biomarkers such as CK-MB and cTn-I for diagnosing myocardial infarction offers high specificity and sensitivity, enabling early and accurate detection of cardiac injury. These biomarkers provide critical insights into the extent of myocardial damage, facilitating timely and targeted clinical interventions. Previous studies have shown that isoproterenol (ISO) promotes cardiac infarction in rodents by the accumulation of CK-MB and cTn-I in the serum, suggesting that it is a well-known model for the development of myocardial infarction (Kannan and Quine 2013, Prince and Roy 2013, Kumar, Kasala et al. 2016). In our study, the ISO-treated group had markedly greater serum levels of CK-MB and cTn-I. Celecoxib treated

group has not shown any significant difference in CK-MB level but it significantly decreased the level of cTn-I. However, as compared to ISO and celecoxib-treated groups, compounds **6c** and **6k** both showed substantially lower CK-MB and cTn-I levels, as reported in Figure 5.8. The advantages of this approach over surgical methods include its convenience, non-invasive procedure, and reduced number of casualties. Since most necrosis occurs in the ventricular subendocardial region and the interventricular septum, the patterns of ischemia necrosis ISO-induced myocardial infarction are comparable to that seen in humans (Kumar, Kasala et al. 2016). Some rats from each group were selected randomly and sacrificed to examine the histopathology of the rat's heart tissue using microscopic examination and the images shown in Figure 5.9. The control group showed normal physiology of the rat heart tissue while it has been observed that the isoproterenol-treated group displayed excessive tissue damage. The synthesized compounds **6c** and **6k** have a resemblance with the control group histopathology indicating no toxic effect of novel drugs in heart tissues. The histological examination of cardiac tissues demonstrated that the synthesized compounds **6c** and **6k** had structural integrity comparable to the control group, with no evidence of cellular damage, inflammation, or necrosis.

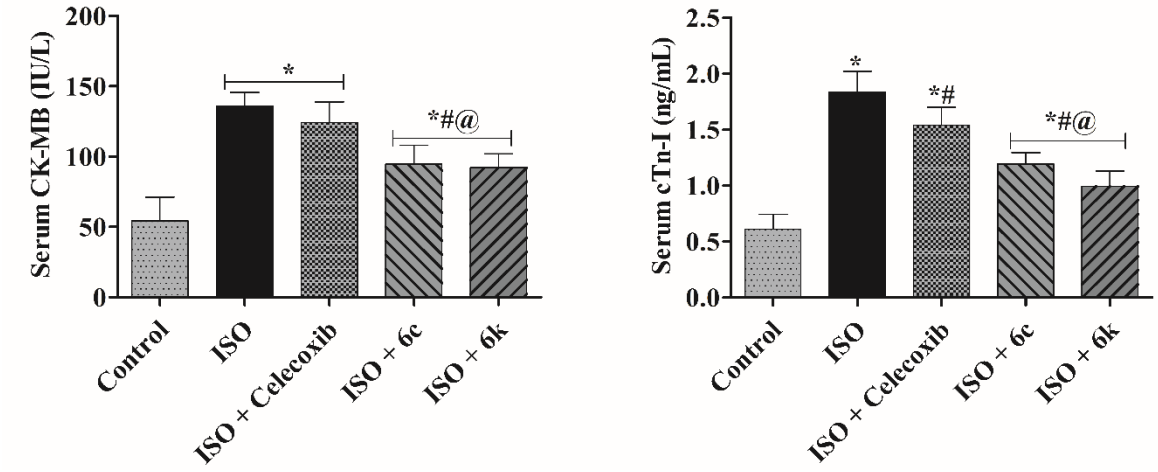

Figure 5.8. All values are represented as mean ± SD, n = 6 rats per group; *p < 0.05 vs. Control (0.3 % sodium CMC mixture in distilled water; 10ml/kg given orally); #p < 0.05 vs. ISO (100 mg/kg given s.c.) in 0.3 % sodium CMC solution; @p < 0.05 vs. ISO + Celecoxib (10 mg/kg

given orally); $ $p < 0.05$ vs. ISO + **6c** (10 mg/kg given orally) in 0.3 % sodium CMC solution; (Repeated measure one-way ANOVA followed by Tukey's test).

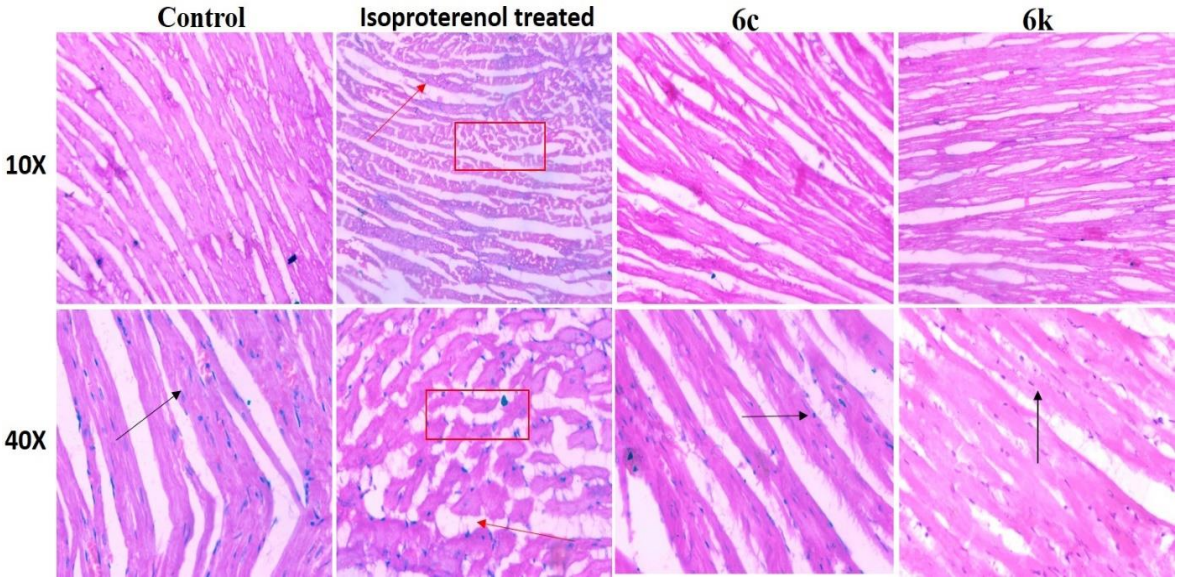

Figure 5.9. Histopathological slides of rat heart (H & E staining): Control group showed normal physiology of heart; Isoproterenol-treated group showed excessive tissue damage & dislocation of nuclei (red box & red arrow); Tested compounds **6c** & **6k** histology revealed normal tissue framework & intact nuclei**.**

This study suggests that the novel compounds do not cause cardiotoxicity, even at therapeutic dosages. The absence of pathological changes in myocardial architecture shows that they are safe for cardiac tissues, which is an important factor to consider when developing anti-inflammatory or therapeutic medicines. These findings highlight the possibility of **6c** and **6k** as safe candidates for future pharmacological research.

5.2. PART-II

NOVEL COMPOUNDS SERIES-II

5.2.1. Computational studies and design consideration

The structure-based drug design approach was utilized and 59,090 piperazine-containing ligands from the ChEMBL database (https://www.ebi.ac.uk/chembl/, accessed on April 2022) were screened using the crystal structure of COX-2 (PDB code: 3LN1) (Kumar, Kasala et al. 2016). Initially, the grid was prepared and validated by re-docking the co-crystallized ligand into the COX-2 protein target. The superimposition tool confirmed the RMSD within the 2Å limit. The VS workflow involved three steps: High Throughput Virtual screening (HTVS), Standard Precision (SP), and Extra Precision (XP) docking with criteria of screening 30% ligands in each of the steps, a total of 28 hits identified as promising COX-2 inhibitors. The top two hits; ChEMBL342253 and ChEMBL4794855 displayed the common presence of benzhydrylpiperazine. Although the hit compounds displayed favorable docking results for the COX-2 enzyme showing favorable hydrophobic interaction with the binding pocket residues such as Ala513, Tyr371, Val509, Met508, Phe504, and Val102 which are similar to the interaction of selective COX-2 inhibitor, celecoxib (Figure 5.10), they did not demonstrate potential binding against the 5-LOX enzyme when compared with the standard, zileuton (Figure 5.11).

It failed to exhibit acceptable molecular stability in dynamic simulation studies. The RMSD graph shown in Figure 5.12 depicted that the hit obtained from the CHEMBL database did not exhibit RMSD within the acceptable range of 1-3 Å. Moreover, the hit did not show favourable interactions with some important amino acid residues which are essential for the activity. Thus, the hit was further modified to develop novel molecules to enhance the stability of the docked molecules in a molecular dynamic simulation run. Interaction with the active site amino acid residues were minimal in the hit

ChEMBL342253, while the designed molecule displayed favourable interactions which are important for the overall stability of the inhibitors in the active site of the COX-2 enzyme.

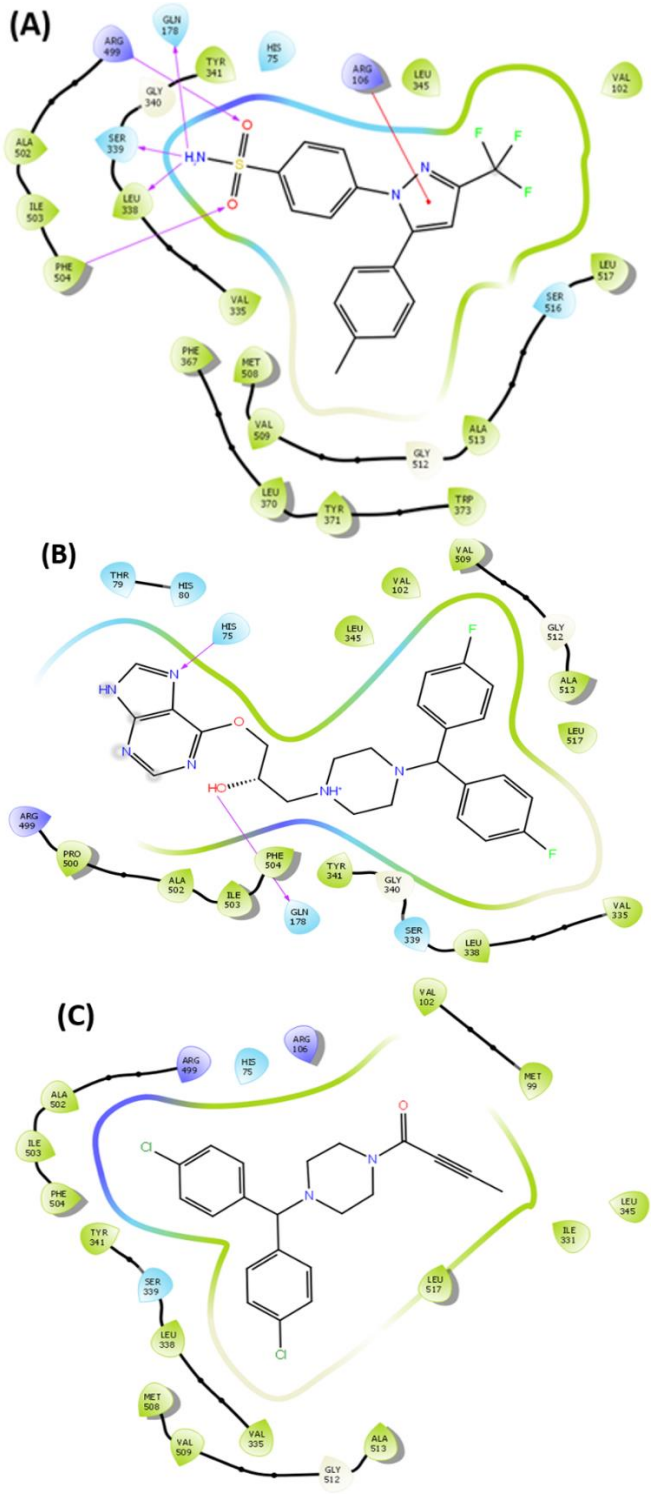

Figure 5.10. 2-D docking poses PDB Id- 3LN1: (A) Celecoxib (B) Hit 1 ChEMBL342253 (C) Hit 2 ChEMBL4794855

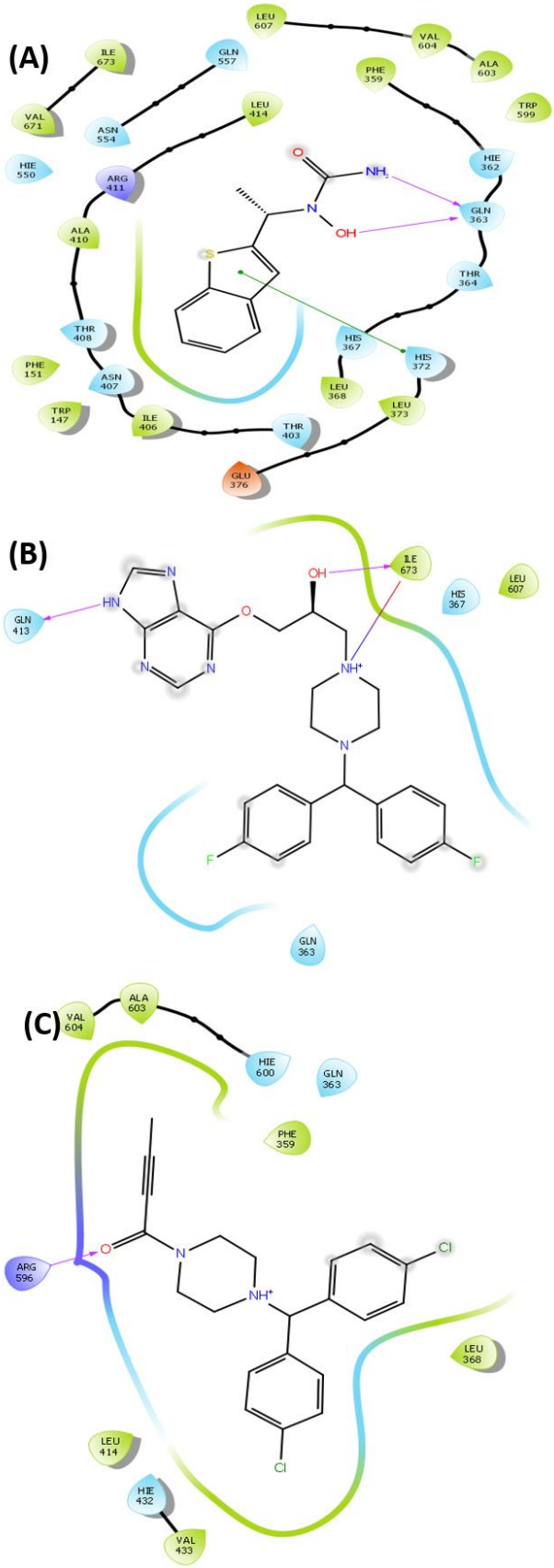

Figure 5.11. 2-D docking poses PDB Id- 6N2W: (A) Zileuton (B) Hit 1 ChEMBL342253 (C) Hit 2 ChEMBL4794855

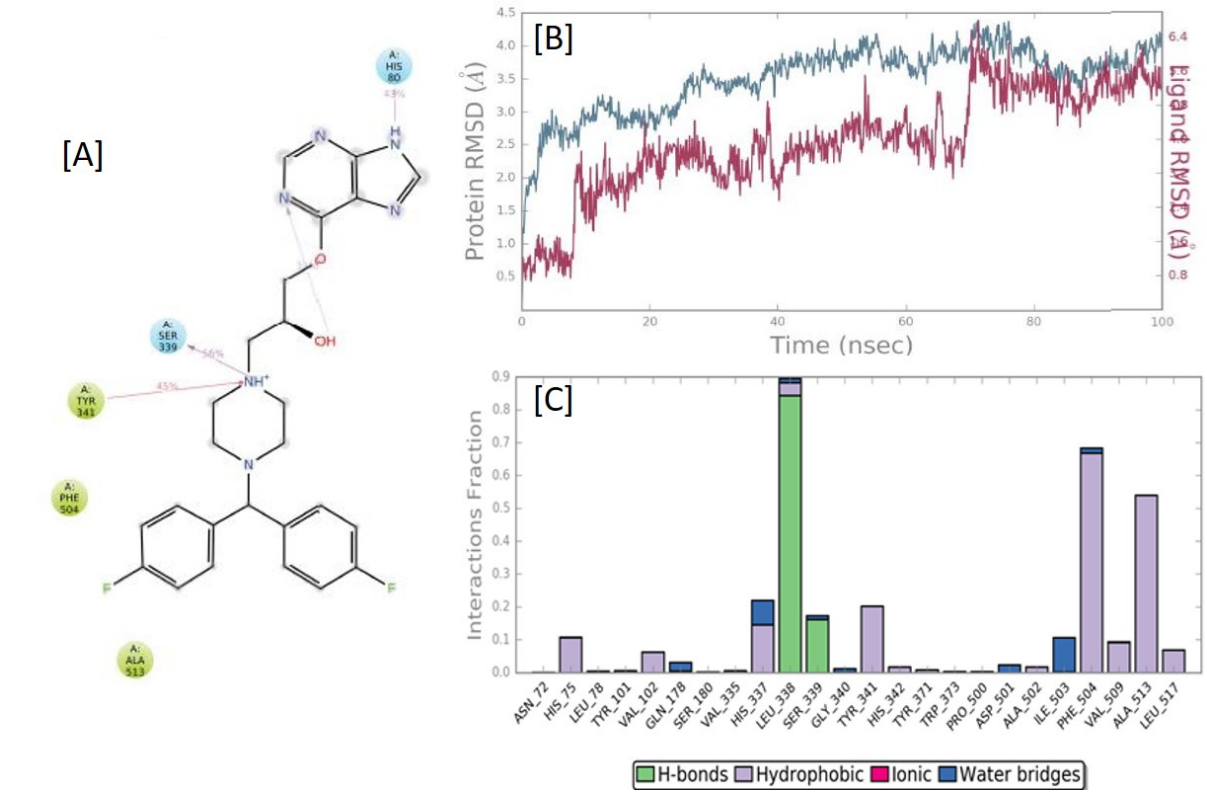

Figure 5.12. MD Simulation studies of screened hit compound ChEMBL342253-COX-2 (3LN1) docked complex: [A] 2D-representation showing percent interaction with active site amino acid residues; [B] RMSD graph of ChEMBL342253 for 100ns run; [C] Histogram depicting interaction between ChEMBL342253 and protein.

The second hit obtained from the ChEMBL database (ChEMBL4794855) was evaluated for molecular stability and binding efficacy to the target protein. However, the results indicated poor stability, as reflected by an RMSD value exceeding the acceptable range of 1–3 Å, suggesting significant conformational deviations during molecular dynamics simulations (Figure 5.13). Furthermore, the molecule failed to establish favorable interactions with key amino acid residues in the active site, essential for strong and specific binding. The absence of critical interactions, such as hydrogen bonding or hydrophobic contacts, undermines its potential as a viable lead compound, necessitating its exclusion from further development or optimization efforts. While, in contrast to this, the designed molecule displayed molecular stability and interactions with the important amino acid residues required for the activity of the inhibitor molecules.

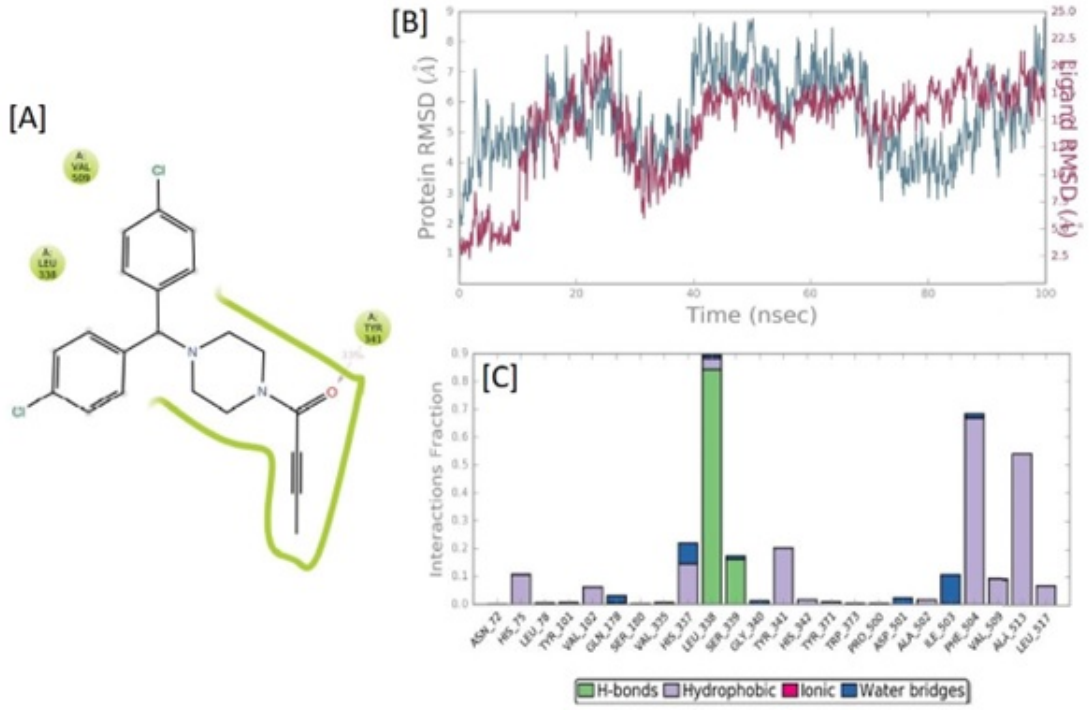

Figure 5.13. MD Simulation studies of ChEMBL4794855-COX-2 (3LN1) docked complex: [A] 2D-representation showing percent interaction with active site amino acid residues; [B] RMSD graph of ChEMBL4794855 for 100ns run; [C] Histogram depicting interaction between ChEMBL342253 and protein.

The molecular hybridization approach was further employed to develop multifunctional ligands with improved molecular binding and stability against both COX-2 and 5-LOX enzymes by incorporating the pharmacophoric features of some known compounds, including hit molecules. The biphenyl rings are usually evident in coxibs, such as celecoxib, as they are necessary to bind the active COX-2 pocket. This characteristic is also evident in licofelone, a dual COX/LOX inhibitor. The hit compounds from the ChEMBL database shared similarities with the scaffold found in licofelone and antihistamines, such as levocetirizine and hydroxyzine. Thus, considering several therapeutic benefits of the scaffold, it is retained in the designed molecules. Subsequently, 1,3,4-oxadiazole was selected as an auxiliary scaffold considering its multifunctional potential (Valente, Trisciuoglio et al. 2014, Dhawan, Kerru et al. 2018, Bashir, Riaz et al. 2022). We identified dual COX-2/5-LOX inhibitory potential in recently developed

molecular hybrids containing 1,3,4-oxadiazole (A). Also, the experimental drug zibotentan, containing 1,3,4-oxadiazole is under investigation for its anti-cancer activity (Miller, Moul et al. 2013, Valente, Trisciuoglio et al. 2014, Wang, Sun et al. 2022). Consequently, the anti-cancer potential of the proposed compounds was also predicted. Based on the aforementioned information, a novel series of molecular hybrids has been developed, and their molecular binding and stability were confirmed through *in-silico* studies.

5.2.1.1. Molecular docking studies of novel compound against COX-2 and 5-LOX

The designed compounds exhibited encouraging glide and dock scores with improved molecular binding into respective grids of COX-2 and 5-LOX. The docking results (Table 5.6) on the COX-2 grid indicated that compound **9d** displayed the docking score of -10.83 which is comparable with the docking score of celecoxib -12.63. The promising compound **9d** showed favorable hydrophobic interaction with the binding pocket residues such as Ala513, Tyr371, Val509, Met508, Phe504, and Val102, which are similar to the interaction of selective COX-2 inhibitor, celecoxib (Figure 5.14). Similarly, the docking result of compound **9d** on the 5-LOX grid showed a better docking score of -5.85 than the standard zileuton with docking scores of -5.28, confirming **9d** binding with both COX-2/5-LOX enzymes.

Table 5.6. Docking scores of the compounds and standard (A) COX-2 and (B) 5-LOX

	Compounds	**Docking Scores on**	
S.No.		**COX-2 (PDB:3LN1)**	**5-LOX (PDB: 6N2W)**
1.	**9d**	-10.830	-5.859
2.	**9g**	-8.440	-4.372
3.	**Celecoxib**	-12.636	NA
4.	**Zileuton**	NA	-5.287

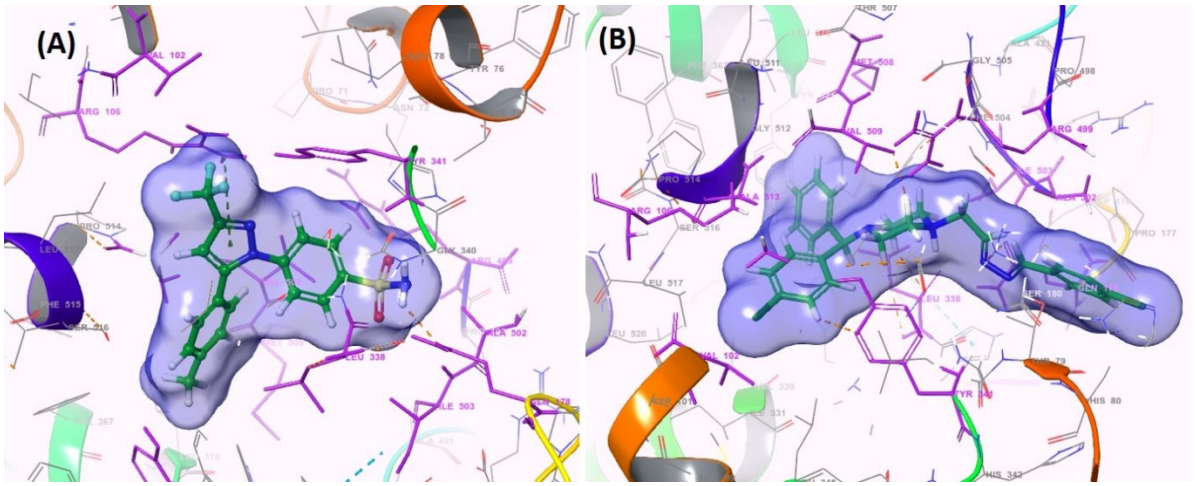

Figure 5.14. 3-D docking poses PDB Id-3LN1: (A) Celecoxib (B) Compound **9d**

The binding mode of docked compounds on the 5-LOX grid (PDB code: 6N2W) displayed that the compound **9d** is well occupied on 5-LOX enzymatic cleft and showed interaction with active site residues such as His367, His372, Gln363, Gln557, and Asn407. His372 showed additional π-π stacking, π-cation interactions, and Ile406, Ile673, Leu607, and Gln363 indicated significant hydrophobic interactions (Figure 5.15). The analysis of binding interactions confirms the active site binding of the synthesized compound, demonstrating its ability to establish key molecular interactions with critical residues of the target enzyme. This further evidence demonstrates the compound's potential as a targeted inhibitor, paving the way for future therapeutic development.

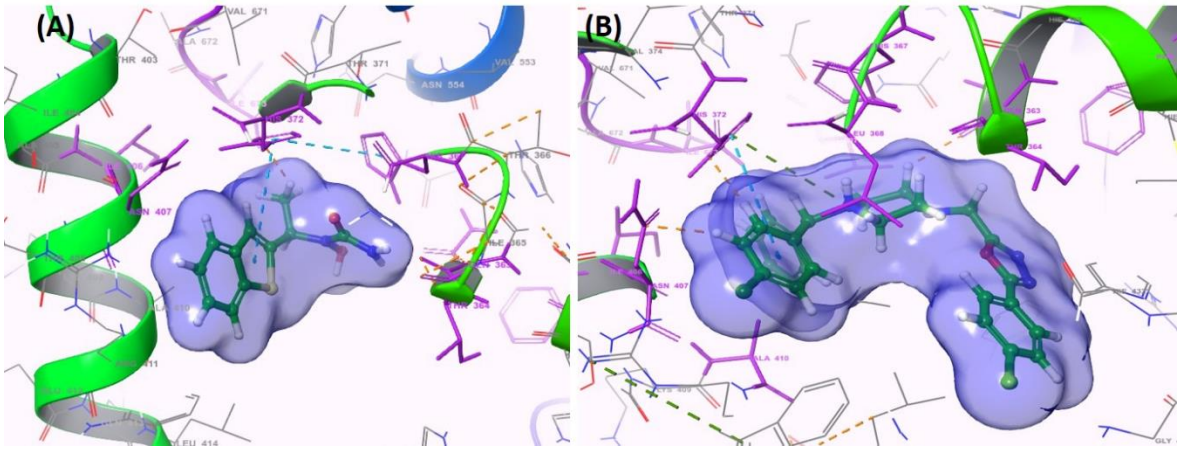

Figure 5.15. 3-D docking poses PDB Id- 6N2W: (A) Zileuton (B) Compound **9d**

5.2.1.2.Molecular dynamics simulation studies of novel compound against COX-2 and 5-LOX

The stability of the docked poses was evaluated through 100ns molecular dynamics (MD) simulation run for **9d** on both the targets COX-2 and 5-LOX. The outcomes of molecular dynamics investigations on COX-2 revealed that derivative **9d** showed favorable interactions with the key residues including hydrogen bonding interaction with Leu338. The hydrophobic interaction was observed for Phe504 and Ala513, which were crucial for the binding and stabilization of inhibitors in the COX-2 active site (Ullah, Khan et al. 2023). The protein-ligand RMSD value was found within the acceptable limit of 1-3 Å for 100 ns simulated trajectory Figure 5.16.

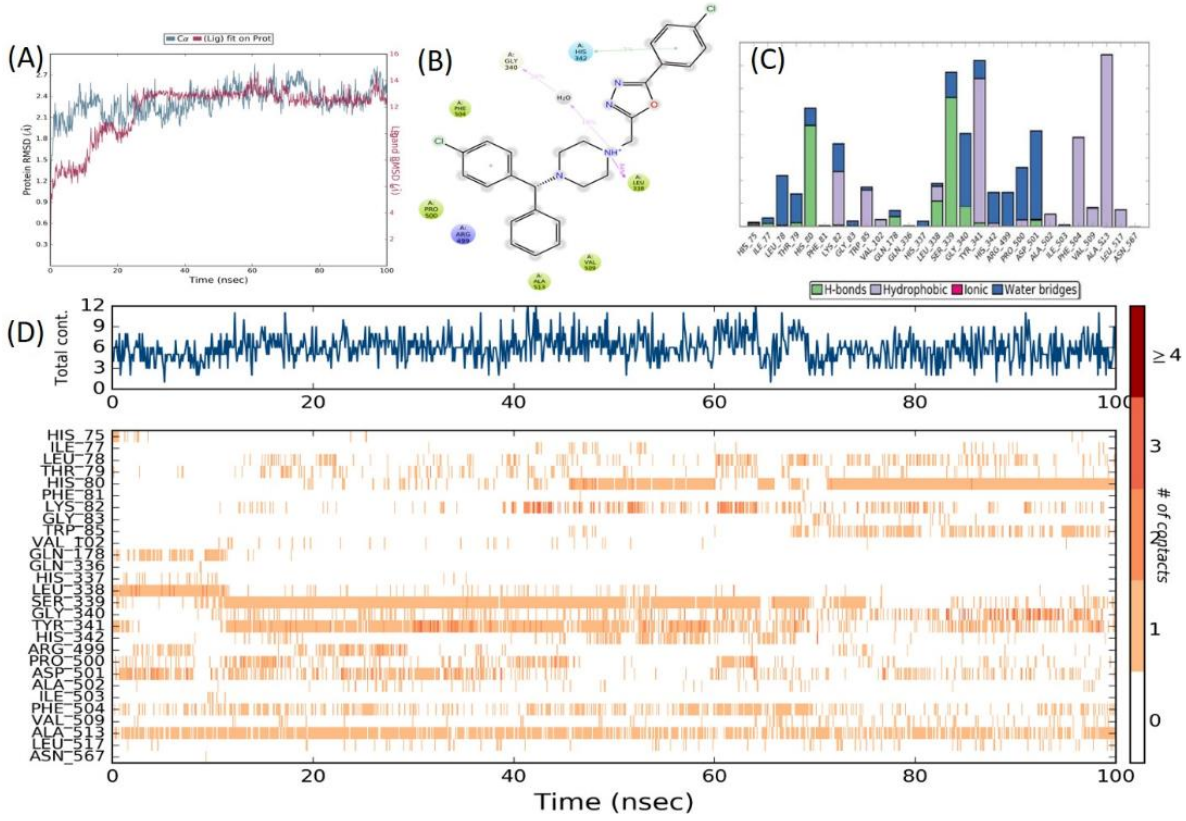

Figure 5.16. MD Simulation studies of 9d-COX-2 (3LN1) docked complex [A] RMSD graph of 9d for 100ns run; [B] 2D-representation showing percent interaction with active site amino acid residues; [C] Histogram depicting interaction between 9d and protein; [D] Timeline representation of interactions with all amino acid residues at each time frame.

The molecular dynamics simulation of 9d on 5-LOX indicated significant hydrophobic interactions with the crucial amino acid residues His367, His372, Ile406, and Ala410. The protein-ligand depicted stable alignment throughout the 100ns simulation run. Furthermore, the docked complex exhibited a strong hydrogen bonding interaction with the Ile673, which is the main carboxylate of the C-terminus of the 5-LOX structural framework *(Gilbert, Bartlett et al. 2011)*. The timeline representation also indicated that the interactions of important amino acid residues were constant throughout each time frame during the MD simulation run (Figure 5.17). The results of molecular dynamic simulations affirm our belief that the designed compound could possess multitarget potential and might be explored in other inflammatory targets.

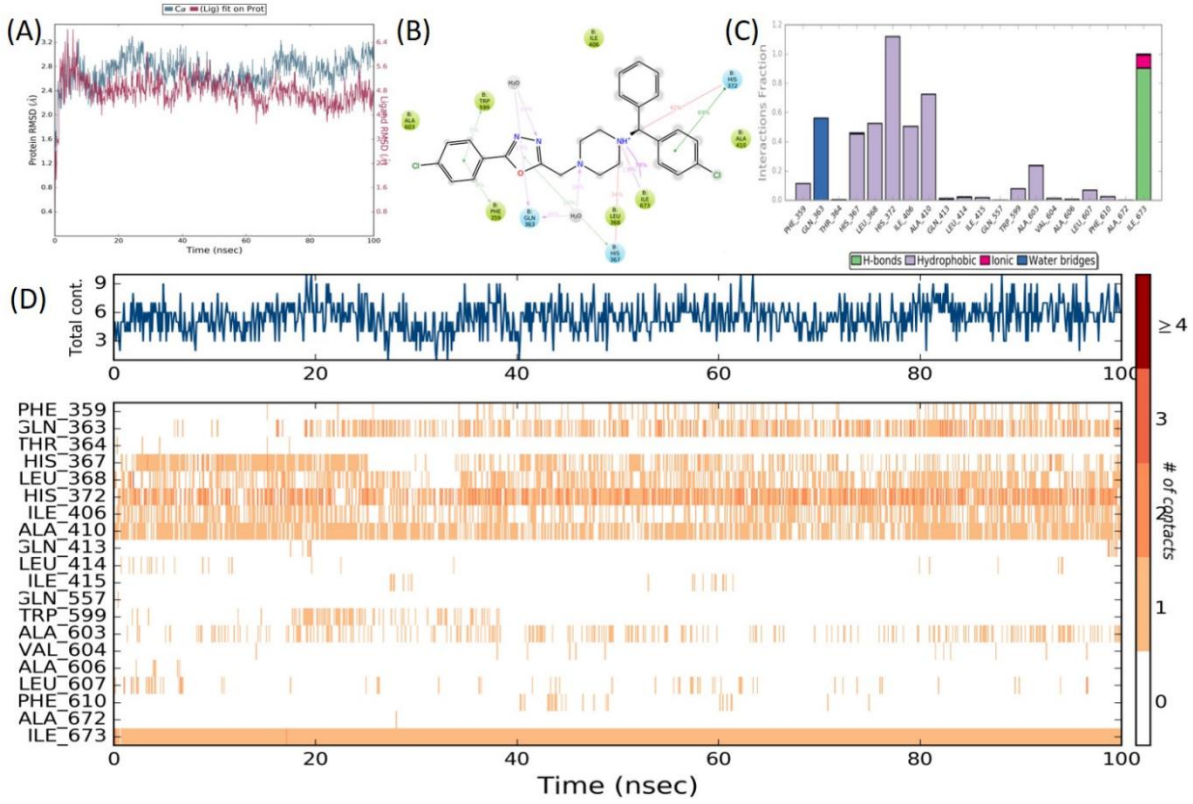

Figure 5.17. MD Simulation studies of 9d-5-LOX (6N2W) docked complex [A] RMSD graph of 9d for 100ns run; [B] 2D-representation showing percent interaction with active site amino acid residues; [C] Histogram depicting interaction between 9d and protein; [D] Timeline representation of interactions with all amino acid residues at each time frame.

Further analysis using the molecular mechanics-generalized born surface area (MM-GBSA) approach was conducted to evaluate the binding free energy of the designed compounds, providing insights into their binding affinity and stability with target enzymes. Among the tested compounds, hit compound **9d** emerged as the most promising candidate, exhibiting minimum binding free energies of -36.628 kcal/mol and -48.307 kcal/mol for the COX-2 and 5-LOX enzymes, respectively, as presented in Table 5.7. These values indicate a strong and favorable interaction between compound **9d** and the active sites of both enzymes. The dual-target activity of **9d** suggests its potential as an effective dual COX-2/5-LOX inhibitor, with significant therapeutic implications for the treatment of inflammatory conditions. These findings highlight **9d** as a lead compound for further optimization and *in vivo* validation.

Table 5.7. MM-GBSA analysis of compound 9d with COX-2 and 5-LOX enzymes

Enzyme targets	Compounds	ΔG binding free energy
COX-2	Celecoxib	-41.416
	9d	-36.628
5-LOX	Zileuton	-44.286
	9d	-48.907

5.2.2. Chemistry

5.2.2.1. Synthesis of novel compounds series II

The series of designed novel molecular hybrids (**9a-u)** were synthesized by connecting benzhydrylpiperazine and substituted phenyl oxadiazoles with $–CH_2$ linker. In brief, boc-piperazine first reacted with 1-chloro-4-(chloro(phenyl)methyl)benzene **(3)** to obtain benzhydrylpiperazine **(5)**. In another reaction, benzoic acid esters were obtained by reacting substituted benzoic acids (**6a-u)** with hydroxybenzotriazole (HOBT) and 1-ethyl-3-(3-dimethylaminopropyl) carbodiimide (EDCI) in acetonitrile (ACN), which

eventually reacted with hydrazine hydrate to yield benzoic acid hydrazides (**7a-u**). Thereafter, benzoic acid hydrazides (**7a-u**) were converted into oxadiazole derivatives (**8a-u)** in a cyclization reaction.

The ^{1}H NMR spectra confirmed the formation of **8a-u** by showing the presence of methylene protons singlet in the δ_H = 4.01-5.11 ppm range; which is also affirmed by the presence of signals at the range of δc = 3.91-4.21 ppm in ^{13}C NMR spectra. In the final reaction, **8a-u** reacted with benzhydrylpiperazine **(5)** with potassium hydroxide (KOH) in solvent dimethylformamide (DMF) via nucleophilic substitution reaction to yield corresponding target compounds (**9a-u)**. In the ^{1}H NMR spectra, the disappearance of the -N**H** proton of benzhydrylpiperazine **(5)** confirmed final product formation (**9a-u)** and was verified by the ^{13}C NMR spectra. The ^{13}C NMR spectra displayed a signal in the range δc = 52.90-55.48 ppm for N–**C**H_2. The high-resolution mass spectrometry (HRMS) also confirmed the molecular weights of all synthesized derivatives. Additionally, the purity of the synthesized derivatives has also been verified by high-performance liquid chromatography (HPLC).

5.2.2.2. Characterization of synthesized derivatives

2-((4-((4-chlorophenyl)(phenyl)methyl)piperazin-1-yl)methyl)-5-(3-methoxy phenyl)-1,3,4-oxadiazole (9a)

Light brown solid, yield 74%; mp 258-259°C; TLC (Hexane/EtOAc 80:20 v/v); ^{1}H NMR (500 MHz, $CDCl_3$) δ 7.98 (t, *J* = 7.5 Hz, 1H), 7.54 – 7.41 (m, 4H), 7.39 (d, *J* = 7.1 Hz, 2H), 7.36 – 7.24 (m, 5H), 7.03 (dt, *J* = 7.5, 1.5 Hz, 1H), 4.23 (s, 1H), 3.80 (s, 2H), 3.82 (s, 3H), 2.64 (s, 4H), 2.41 (s, 4H); ^{13}C NMR (125 MHz, $CDCl_3$) δ 166.14, 163.80, 162.11, 141.54, 139.07, 134.44, 129.22, 129.14, 128.96, 128.46, 128.41, 127.71, 127.26, 119.57, 117.36, 116.11, 75.37, 55.52, 52.96, 51.33, 51.12; HRMS $[M+1]^+$ Calculated 475.1895, Found 475.1884; HPLC Purity: 96.71%, Retention time: 4.39 min.

2-((4-((4-chlorophenyl)(phenyl)methyl)piperazin-1-yl)methyl)-5-(4-methoxyphenyl)-1,3,4-oxadiazole (9b)

Light brown solid, yield 76%; mp 257-258°C; TLC (Hexane/EtOAc 80:20 v/v); ^{1}H NMR (500 MHz, $CDCl_3$) δ 8.06 (d, *J* = 8.9 Hz, 2H), 8.00 (d, *J* = 8.9 Hz, 2H), 7.34 (s, 4H), 7.19 (d, *J* = 7.2 Hz, 1H), 7.03 (d, *J* = 8.9 Hz, 2H), 7.00 (d, *J* = 8.9 Hz, 2H), 4.21 (s, 1H), 3.89 (s, 2H), 3.88 (s, 3H), 2.66 (s, 4H), 2.44 (s, 4H); ^{13}C NMR (125 MHz, $CDCl_3$) δ 165.32, 164.12, 162.74, 162.39, 162.23, 129.19, 128.94, 128.79, 128.71, 128.65, 128.60, 127.84, 127.26, 116.63, 116.32, 114.60, 114.50, 114.47, 75.33, 55.48, 52.91, 51.80, 51.56; HRMS $[M+1]^+$ Calculated 475.1895, Found 475.1886; HPLC Purity: 97.58%, Retention time: 4.36 min.

2-(3-chlorophenyl)-5-((4-((4-chlorophenyl)(phenyl)methyl)piperazin-1-yl)methyl)-1,3,4-oxadiazole (9c)

Light brown solid, yield 81%; mp 262-264°C; TLC (Hexane/EtOAc 80:20 v/v); ^{1}H NMR (500 MHz, $CDCl_3$) δ 8.05 (s, 1H), 7.96 (d, *J* = 7.8 Hz, 1H), 7.51 (d, *J* = 7.9 Hz, 1H), 7.44 (t, *J* = 8.0 Hz, 1H), 7.34 (dd, *J* = 7.0, 4.8 Hz, 5H), 7.25 – 7.17 (m, 4H), 4.22 (s, 1H), 3.90 (s, 2H), 2.65 (s, 4H), 2.40 (s, 4H); ^{13}C NMR (125 MHz, $CDCl_3$) δ 164.26, 163.67, 141.93, 141.13, 135.22, 132.64, 131.84, 130.43, 129.23, 129.17, 128.70, 128.64, 127.89, 127.82, 127.25, 127.00, 125.44, 125.11, 75.29, 53.02, 51.84, 51.52; HRMS $[M+1]^+$ Calculated 479.1400, Found 479.1390; HPLC Purity: 96.11%, Retention time: 4.85 min.

2-(4-chlorophenyl)-5-((4-((4-chlorophenyl)(phenyl)methyl)piperazin-1-yl)methyl)-1,3,4-oxadiazole (9d)

Light brown solid, yield 84%; mp 263-264°C; TLC (Hexane/EtOAc 80:20 v/v); ^{1}H NMR (500 MHz, $CDCl_3$) δ 8.00 (d, *J* = 8.3 Hz, 2H), 7.49 (d, *J* = 8.3 Hz, 2H), 7.33 (d, *J* = 5.5 Hz, 5H), 7.21 (dd, *J* = 20.1, 7.8 Hz, 4H), 4.22 (s, 1H), 3.89 (s, 2H), 2.65 (s, 4H), 2.44 (s,

4H); ^{13}C NMR (125 MHz, $CDCl_3$) δ 164.58, 163.50, 141.91, 141.11, 138.10, 132.65, 129.55, 129.44, 129.17, 128.69, 128.62, 128.29, 128.23, 127.82, 127.24, 122.32, 75.29, 53.03, 51.84, 51.53; HRMS $[M+1]^+$ Calculated 479.1400, Found 479.1407; HPLC Purity: 96.81%, Retention time: 4.88 min.

2-((4-((4-chlorophenyl)(phenyl)methyl)piperazin-1-yl)methyl)-5-(2,4-dichlorophenyl)-1,3,4-oxadiazole (9e)

Brown solid, yield 78%; mp 259-261°C; TLC (Hexane/EtOAc 80:20 v/v); ^{1}H NMR (500 MHz, $CDCl_3$) δ 7.96 (d, *J* = 8.4 Hz, 1H), 7.60 (d, *J* = 1.2 Hz, 1H), 7.42 (dd, *J* = 8.4, 1.4 Hz, 1H), 7.36 (dd, *J* = 7.3, 4.8 Hz, 4H), 7.29 (d, *J* = 7.4 Hz, 3H), 7.21 (dd, *J* = 17.0, 9.7 Hz, 2H), 4.24 (s, 1H), 3.96 (s, 2H), 2.69 (s, 4H), 2.43 (s, 4H); ^{13}C NMR (125 MHz, $CDCl_3$) δ 164.00, 163.02, 141.95, 141.14, 138.23, 133.96, 132.64, 131.97, 131.16, 129.16, 129.09, 128.89, 128.82, 128.71, 128.65, 127.81, 127.76, 127.64, 127.25, 121.71, 75.28, 52.92, 51.74, 51.56; HRMS $[M+1]^+$ Calculated 513.1010, Found 513.1051; HPLC Purity: 96.24%, Retention time: 4.96 min.

2-(4-chloro-3-nitrophenyl)-5-((4-((4-chlorophenyl)(phenyl)methyl)piperazin-1-yl)methyl)-1,3,4-oxadiazole (9f)

Dark brown solid, yield 82%; mp 256-258°C; TLC (Hexane/EtOAc 80:20 v/v); ^{1}H NMR (500 MHz, $CDCl_3$) δ 8.42 (d, *J* = 1.4 Hz, 1H), 8.31 (dd, *J* = 7.5, 1.6 Hz, 1H), 8.18 (d, *J* = 7.5 Hz, 1H), 7.39 – 7.21 (m, 9H), 4.25 (s, 1H), 3.88 (s, 2H), 2.66 (s, 4H), 2.46 (s, 4H); ^{13}C NMR (125 MHz, $CDCl_3$) δ 168.11, 165.41, 150.25, 142.88, 142.01, 132.69, 130.22, 129.27, 129.21, 129.16, 129.13, 128.91, 128.78, 128.64, 126.10, 124.83, 76.16, 52.88, 51.71, 51.49; HRMS $[M+1]^+$ Calculated 524.1251, Found 524.1203; HPLC Purity: 95.16%, Retention time: 5.15 min.

2-((4-((4-chlorophenyl)(phenyl)methyl)piperazin-1-yl)methyl)-5-(4-nitrophenyl)-1,3,4-oxadiazole (9g)

Dark brown solid, yield 86%; mp 258-259°C; TLC (Hexane/EtOAc 80:20 v/v); ^{1}H NMR (500 MHz, $CDCl_3$) δ 8.39 (d, *J* = 8.6 Hz, 2H), 8.28 (d, *J* = 8.6 Hz, 2H), 7.36 (dd, *J* = 6.9, 4.8 Hz, 5H), 7.29 (s, 2H), 7.25 – 7.21 (m, 2H), 4.24 (s, 1H), 3.95 (s, 2H), 2.69 (s, 4H), 2.44 (s, 4H); ^{13}C NMR (125 MHz, $CDCl_3$) δ 164.45, 163.68, 149.63, 141.86, 141.06, 132.67, 129.28, 129.20, 129.16, 128.72, 128.66, 128.12, 127.97, 127.85, 127.81, 127.28, 124.59, 124.38, 75.28, 53.13, 51.88, 51.50; HRMS $[M+1]^+$ Calculated 490.1640, Found 490.1640; HPLC Purity: 98.65%, Retention time: 4.30 min.

2-((4-((4-chlorophenyl)(phenyl)methyl)piperazin-1-yl)methyl)-5-(3,5-dinitro phenyl)-1,3,4-oxadiazole (9h)

Dark brown solid, yield 81%; mp 255-257°C; TLC (Hexane/EtOAc 80:20 v/v); ^{1}H NMR (500 MHz, $CDCl_3$) δ 8.86 (t, *J* = 1.4 Hz, 1H), 7.79 (d, *J* = 1.4 Hz, 2H), 7.41 – 7.16 (m, 9H), 4.51 (s, 1H), 3.99 (s, 2H), 2.72 (s, 4H), 2.51 (s, 4H); ^{13}C NMR (125 MHz, $CDCl_3$) δ 169.74, 162.11, 149.44, 140.28, 139.64, 132.14, 129.85, 129.71, 129.43, 128.22, 128.01, 127.24, 126.17, 119.68, 76.11, 52.22, 51.78, 51.46; HRMS $[M+1]^+$ Calculated 535.1491, Found 535.1454; HPLC Purity: 95.15%, Retention time: 5.13 min.

2-((4-((4-chlorophenyl)(phenyl)methyl)piperazin-1-yl)methyl)-5-(2,4-difluoro phenyl)-1,3,4-oxadiazole (9i)

^{1}H NMR (500 MHz, $CDCl_3$) δ 8.03 (dt, *J* = 7.4, 5.0 Hz, 1H), 7.88 (dd, *J* = 7.5, 1.4 Hz, 2H), 7.29 (dd, *J* = 14.1, 4.4 Hz, 5H), 7.26 (d, *J* = 1.4 Hz, 1H), 7.22 – 7.19 (m, 1H), 7.02 – 6.88 (m, 2H), 4.29 (s, 1H), 3.96 (s, 2H), 2.69 (s, 4H), 2.48 (s, 4H); ^{13}C NMR (125 MHz, $CDCl_3$) δ 169.38, 165.88, 165.47, 164.93, 164.88, 163.23, 163.11, 162.21, 162.14, 154.61, 154.12, 141.88, 141.81, 139.17, 132.16, 130.81, 130.79, 129.22, 129.18, 128.12,

128.09, 116.44, 116.41, 116.38, 116.36, 114.11, 114.04, 105.68, 105.66, 105.63, 75.33, 53.18, 51.55, 51.19; HRMS $[M+1]^+$ Calculated 481.1601, Found 481.1669; HPLC Purity: 96.33%, Retention time: 4.81 min.

2-((4-((4-chlorophenyl)(phenyl)methyl)piperazin-1-yl)methyl)-5-(2,4,5-trifluoro phenyl)-1,3,4-oxadiazole (9j)

^{1}H NMR (500 MHz, $CDCl_3$) δ 7.99 (ddd, *J* = 7.9, 5.6, 2.1 Hz, 3H), 7.67 (dd, *J* = 12.5, 6.2 Hz, 6H), 7.29 – 7.22 (m, 1H), 6.91 (td, *J* = 8.1, 5.0 Hz, 1H), 4.18 (s, 1H), 3.97 (s, 2H), 2.65 (s, 4H), 2.44 (s, 4H); ^{13}C NMR (125 MHz, $CDCl_3$) δ 170.01, 168.94, 163.91, 163.18, 159.85, 157.85, 157.81, 157.79, 157.76, 153.78, 153.75, 152.93, 152.87, 150.81, 150.76, 148.81, 148.78, 148.59, 148.55, 146.71, 146.68, 140.56, 139.07, 132.44, 129.90, 129.74, 128.39, 126.73, 116.26, 116.01, 113.94, 113.63, 113.56, 113.32, 106.43, 106.38, 105.88, 105.81, 75.41, 52.81, 51.58, 51.23; HRMS $[M+1]^+$ Calculated 499.1507, Found 499.1438; HPLC Purity: 94.93%, Retention time: 4.90 min.

2-((4-((4-chlorophenyl)(phenyl)methyl)piperazin-1-yl)methyl)-5-(4-(trifluoro methoxy)phenyl)-1,3,4-oxadiazole (9k)

^{1}H NMR (500 MHz, $CDCl_3$) δ 7.80 (d, *J* = 7.5 Hz, 2H), 7.62 – 7.28 (m, 9H), 7.01 (d, *J* = 7.5 Hz, 2H), 4.17 (s, 1H), 3.93 (s, 2H), 2.62 (s, 4H), 2.46 (s, 4H). ^{13}C NMR (125 MHz, $CDCl_3$) δ 172.00, 164.09, 152.13, 152.06, 151.89, 151.63, 140.22, 138.06, 132.04, 129.88, 129.72, 129.31, 128.38, 126.69, 125.04, 123.61, 122.94, 120.73, 120.45, 120.31, 120.27, 120.25, 118.74, 75.58, 52.91, 52.64, 50.12; HRMS $[M+1]^+$ Calculated 529.1613, Found 529.1569; HPLC Purity: 95.41%, Retention time: 4.61 min.

2-((4-((4-chlorophenyl)(phenyl)methyl)piperazin-1-yl)methyl)-5-(4-fluorophenyl)-1,3,4-oxadiazole (9l)

^{1}H NMR (500 MHz, $CDCl_3$) δ 8.08 (dd, *J* = 8.7, 5.2 Hz, 2H), 7.36 (dd, *J* = 7.5, 5.2 Hz, 4H), 7.28 (d, *J* = 7.3 Hz, 2H), 7.25 – 7.21 (m, 3H), 7.21 – 7.18 (m, 2H), 4.24 (s, 1H), 3.91 (s, 2H), 2.67 (s, 4H), 2.46 (s, 4H); ^{13}C NMR (125 MHz, $CDCl_3$) δ165.83, 164.57, 163.82, 163.35, 141.93, 141.14, 132.63, 129.35, 129.28, 129.18, 128.69, 128.64, 127.83, 127.24, 120.17, 116.48, 116.30, 75.29, 53.01, 51.84, 51.54; HRMS $[M+1]^+$ Calculated 463.1695, Found 463.1733; HPLC Purity: 96.47%, Retention time: 4.44 min.

2-((4-((4-chlorophenyl)(phenyl)methyl)piperazin-1-yl)methyl)-5-(2-nitrophenyl)-1,3,4-oxadiazole (9m)

^{1}H NMR (500 MHz, $CDCl_3$) δ 8.37 (dd, *J* = 7.5, 1.4 Hz, 1H), 8.29 (dd, *J* = 8.9, 7.5, 1.4 Hz, 1H), 7.47 (td, *J* = 7.4, 1.5 Hz, 1H), 7.39 (td, *J* = 7.4, 1.5 Hz, 1H), 7.34 – 7.22 (m, 9H), 4.26 (s, 1H), 3.98 (s, 2H), 2.66 (s, 4H), 2.46 (s, 4H); ^{13}C NMR (125 MHz, $CDCl_3$) δ 165.38, 164.17, 150.59, 141.66, 141.04, 133.72, 130.99, 129.29, 129.18, 128.64, 128.61, 128.10, 127.96, 127.87, 127.82, 127.78, 124.39, 124.52, 75.44, 53.11, 51.82, 51.51; HRMS $[M+1]^+$ Calculated 490.1640, Found 490.1696; HPLC Purity: 96.52%, Retention time: 4.39 min.

3-(5-((4-((4-chlorophenyl)(phenyl)methyl)piperazin-1-yl)methyl)-1,3,4-oxadiazol-2-yl) benzonitrile (9n)

^{1}H NMR (500 MHz, $CDCl_3$) δ 8.10 (t, *J* = 1.3 Hz, 1H), 7.96 – 7.90 (m, 1H), 7.84 – 7.77 (m, 2H), 7.48 – 7.32 (m, 9H), 4.31 (s, 1H), 3.89 (s, 2H), 2.62 (s, 4H), 2.51 (s, 4H); ^{13}C NMR (125 MHz, $CDCl_3$) δ 171.06, 163.11, 141.47, 138.21, 133.44, 133.18, 129.88, 129.83, 129.75, 129.46, 129.41, 128.32, 127.93, 127.71, 127.27, 120.19, 117.33, 75.49, 52.96, 51.16, 51.03; HRMS $[M+1]^+$ Calculated 470.1742, Found 470.1802; HPLC Purity: 95.52%, Retention time: 4.56 min.

4-(5-((4-((4-chlorophenyl)(phenyl)methyl)piperazin-1-yl)methyl)-1,3,4-oxadiazol-2-yl) benzonitrile (9o)

^{1}H NMR (500 MHz, $CDCl_3$) δ 7.98 (d, *J* = 7.4 Hz, 2H), 7.82 (d, *J* = 7.5 Hz, 2H), 7.51 (dd, *J* = 14.7, 5.7 Hz, 5H), 7.47 (dd, *J* = 10.9, 4.5 Hz, 4H), 4.33 (s, 1H), 3.85 (s, 2H), 2.64 (s, 4H), 2.49 (s, 4H); ^{13}C NMR (125 MHz, $CDCl_3$) δ 173.10, 163.42, 14.54, 139.07, 133.34, 123.98, 129.91, 129.73, 129.38, 129.32, 128.31, 127.33, 126.93, 120.16, 114.41, 75.44, 52.87, 51.16, 51.34; HRMS $[M+1]^+$ Calculated 470.1742, Found 470.17.93; HPLC Purity: 95.88%, Retention time: 4.59 min.

2-((4-((4-chlorophenyl)(phenyl)methyl)piperazin-1-yl)methyl)-5-phenyl-1,3,4-oxadiazole (9p)

^{1}H NMR (500 MHz, $CDCl_3$) δ 7.89 (dd, *J* = 7.4, 1.3 Hz, 2H), 7.63 – 7.51 (m, 5H), 7.42 – 7.28 (m, 7H), 4.47 (s, 1H), 3.81 (s, 2H), 2.69 (s, 4H), 2.53 (s, 4H); ^{13}C NMR (125 MHz, $CDCl_3$) δ 176.01, 168.06, 142.76, 140.77, 133.42, 132.56, 129.93, 129.71, 129.33, 129.02, 128.34, 127.17, 126.91, 126.18, 75.18, 52.82, 51.19, 51.31; HRMS $[M+1]^+$ Calculated 445.1790, Found 445.1850; HPLC Purity: 96.12%, Retention time: 4.11 min.

3-(5-((4-((4-chlorophenyl)(phenyl)methyl)piperazin-1-yl)methyl)-1,3,4-oxadiazol-2-yl) phenol (9q)

^{1}H NMR (500 MHz, $CDCl_3$) δ 8.51 (s, 1H), 7.30 –7.25 (m, 5H), 7.24 – 7.17 (m, 5H), 7.13 – 7.06 (m, 2H), 6.85 – 6.80 (m, 1H), 4.49 (s, 1H), 3.64 (s, 2H), 2.74 (s, 4H), 2.56 (s, 4H); ^{13}C NMR (125 MHz, $CDCl_3$) δ 174.00, 164.20, 159.61, 141.56, 139.07, 132.44, 130.91, 129.90, 129.74, 129.33, 128.39, 126.73, 126.15, 121.00, 118.30, 114.24, 76.58, 52.86, 51.18, 50.13; HRMS $[M+1]^+$ Calculated 461.1739, Found 461.1690; HPLC Purity: 93.82%, Retention time: 3.98 min.

4-(5-((4-((4-chlorophenyl)(phenyl)methyl)piperazin-1-yl)methyl)-1,3,4-oxadiazol-2-yl) phenol (9r)

^{1}H NMR (500 MHz, $CDCl_3$) δ 9.17 (s, 1H), 7.43 (d, *J* = 7.5 Hz, 2H), 7.32 – 7.21 (m, 7H), 7.15 (d, *J* = 7.5 Hz, 2H), 7.00 (d, *J* = 7.5 Hz, 2H), 5.19 (s, 1H), 3.61 (s, 2H), 2.66 (s, 4H), 2.45 (s, 4H); ^{13}C NMR (125 MHz, $CDCl_3$) δ 173.00, 163.07, 161.72, 142.56, 139.06, 132.41, 129.90, 129.74, 129.31, 128.39, 127.58, 126.73, 117.41, 115.81, 77.58, 52.84, 52.18, 50.33; HRMS $[M+1]^+$ Calculated 461.1739, Found 461.1696; HPLC Purity: 94.24%, Retention time: 4.21 min.

2-((4-((4-chlorophenyl)(phenyl)methyl)piperazin-1-yl)methyl)-5-(4-(trifluoro methyl)phenyl)-1,3,4-oxadiazole (9s)

^{1}H NMR (500 MHz, $CDCl_3$) δ 7.62 (d, *J* = 7.5 Hz, 2H), 7.51 (d, *J* = 7.5 Hz, 2H), 7.33 – 7.20 (m, 9H), 5.20 (s, 1H), 3.49 (s, 2H), 2.65 (s, 4H), 2.46 (s, 4H); ^{13}C NMR (125 MHz, $CDCl_3$) δ 173.01, 162.08, 141.56, 139.07, 134.27, 132.44, 132.37, 132.16, 129.90, 129.74, 129.33, 128.39, 127.60, 126.73, 126.67, 126.62, 126.57, 126.50, 126.43, 126.40, 126.37, 126.34, 125.51, 123.41, 121.32, 77.54, 52.83, 52.19, 49.39; HRMS $[M+1]^+$ Calculated 513.1664, Found 513.1718; HPLC Purity: 96.46%, Retention time: 4.63 min.

2-((4-((4-chlorophenyl)(phenyl)methyl)piperazin-1-yl)methyl)-5-(m-tolyl)-1,3,4-oxadiazole (9t)

^{1}H NMR (500 MHz, $CDCl_3$) δ 7.69 (dd, *J* = 4.4, 2.8 Hz, 2H), 7.49 (t, *J* = 7.7 Hz, 1H), 7.33 (dd, *J* = 7.6, 1.6 Hz, 2H), 7.31 – 7.25 (m, 6H), 7.24 (d, *J* = 1.6 Hz, 1H), 7.23 (d, *J* = 1.5 Hz, 1H), 5.19 (s, 1H), 3.52 (s, 2H), 2.71 (s, 4H), 2.51 (s, 4H), 2.36 (s, 3H); ^{13}C NMR (125 MHz, $CDCl_3$) δ 173.00, 162.20, 140.55, 139.02, 138.98, 132.44, 131.01, 129.93, 129.76, 128.41, 128.39, 127.89, 126.74, 126.70, 126.51, 77.58, 52.86, 52.18, 49.31,

21.36; HRMS $[M+1]^+$ Calculated 459.1946, Found 459.1898; HPLC Purity: 95.41%, Retention time: 5.55 min.

2-((4-((4-chlorophenyl)(phenyl)methyl)piperazin-1-yl)methyl)-5-(p-tolyl)-1,3,4-oxadiazole (9u)

^{1}H NMR (500 MHz, $CDCl_3$) δ 7.58 (d, *J* = 7.5 Hz, 2H), 7.36 – 7.23 (m, 11H), 5.24 (s, 1H), 3.79 (s, 2H), 2.73 (s, 4H), 2.60 (s, 4H), 2.34 (s, 3H); ^{13}C NMR (125 MHz, $CDCl_3$) δ 173.06, 162.07, 140.60, 140.56, 139.07, 132.44, 129.90, 129.74, 129.33, 129.09, 128.39, 126.98, 126.73, 125.47, 77.52, 52.85, 52.19, 49.33, 21.31; HRMS $[M+1]^+$ Calculated 459.1946, Found 459.1989; HPLC Purity: 95.62%, Retention time: 5.58 min.

5.2.3. Biological screening

5.2.3.1. In Vitro Biological Evaluation

5.2.3.1.1. COX-1 and COX-2 inhibition activities

The colorimetric inhibitor screening assay method was utilized to evaluate the inhibitory potential of the synthesized compounds on COX-1 and COX-2 enzymes {Bano, 2011 #198. Indomethacin and celecoxib were utilized as the reference drugs. A range of submicromolar to low micromolar IC_{50} values were observed for the compounds (Table 5.8). All the compounds displayed COX-2 selectivity, and the most active compounds against COX-2 were **9d**, **9e**, **9g**, and **9l,** with IC_{50} values of 0.25 µM, 0.47 µM, 0.49 µM, and 0.48 µM, respectively. The calculated selectivity index (SI) confirmed the COX-2 selectivity of celecoxib and the synthesized compounds. The compound **9d** with a SI of 133.59 emerged as the most potent COX-2 inhibitor, while indomethacin and celecoxib demonstrated SI values of 0.91 and 82.04 respectively.

Table 5.8. Results of COX-1, COX-2, and 5-LOX inhibitory potential of synthesized compounds

CMP	-R	IC_{50} COX-2 (µM)[a]	IC_{50} COX-1 (µM)[a]	Selectivity Index[b]	IC_{50} 5-LOX (µM)[a]
9a	3-OCH_3	0.66 ± 0.076	36.26 ± 0.993	54.94	15.28 ± 0.219
9b	4-OCH_3	0.54 ± 0.074	34.46 ± 0.755	65.6	10.35 ± 0.110
9c	3-Cl	0.53 ± 0.061	32.03 ± 0.196	60.43	16.23 ± 0.018
9d	4-Cl	**0.25 ± 0.030**	34.07 ± 0.828	133.59	**7.87 ± 0.334**
9e	2,4-diCl	0.47 ± 0.014	30.32 ± 0.414	64.52	14.38 ± 0.630
9f	4-Cl-3-NO_2	0.72 ± 0.021	38.54 ± 0.854	55.11	11.21 ± 0.221
9g	4-NO_2	**0.49 ± 0.012**	41.06 ± 0.214	87.63	**9.16 ± 0.210**
9h	3,5-diNO_2	0.60 ± 0.117	37.73 ± 0.096	62.42	18.04 ± 0.041
9i	2,3-diCl	0.58 ± 0.071	34.76 ± 0.078	59.58	9.33 ± 0.132
9j	2,4,5-triF	0.52 ± 0.053	32.71 ± 0.209	62.72	19.94 ± 0.259
9k	4-OCF_3	0.63 ± 0.075	27.88 ± 0.773	44.6	9.40 ± 0.032
9l	4-F	0.48 ± 0.081	34.19 ± 0.105	71.23	11.64 ± 0.676
9m	2-NO_2	0.74 ± 0.054	29.89 ± 0.046	40.61	13.53 ± 0.043
9n	3-CN	0.63 ± 0.088	23.03 ± 0.429	36.67	15.02 ± 0.146
9o	4-CN	0.59 ± 0.024	25.49 ± 0.131	43.35	13.49 ± 0.202
9p	H	0.61 ± 0.071	38.42 ± 0.398	63.08	9.81 ± 0.201
9q	3-OH	0.73 ± 0.050	36.30 ± 0.015	50.03	20.26 ± 0.105
9r	4-OH	0.66 ± 0.127	36.34 ± 0.447	54.89	10.78 ± 0.277
9s	4-CF_3	0.57 ± 0.027	26.95 ± 0.108	47.03	13.70 ± 0.236
9t	3-CH_3	0.68 ± 0.031	30.71 ± 0.177	44.9	9.89 ± 0.018
9u	4-CH_3	0.70 ± 0.132	32.05 ± 0.267	45.78	18.10 ± 0.270
Celecoxib		0.36 ± 0.023	29.99 ± 0.060	82.04	nd
Zileuton		nd	nd	nd	14.29 ± 0.173
Indomethacin		0.35 ± 0.013	0.32 ± 0.008	0.91	nd

[a]All values are presented as the mean ±SD;
[b]COX-2 selectivity index = IC_{50} of COX-1/IC_{50} of COX-2
[nd]Not determined

5.2.3.1.2. 5-LOX inhibition activity

The 5-LOX inhibitory potential of the synthesized compounds was also investigated. The results revealed that most of the evaluated derivatives were 5-LOX enzyme inhibitors with comparable potency to standard zileuton. Among all the examined derivatives, **9d**

and **9g** demonstrated the highest inhibitory potential with IC_{50} values of 7.87 µM and 9.16 µM respectively, while zileuton displayed an IC_{50} value of 14.29 µM. Upon a closer examination of Table 5.8, noteworthy characteristics of the dual COX-2/5-LOX inhibitory potential of the synthesized compounds become evident.

5.2.3.2. Structure activity relationship (SAR)

The substitution of EDGs at C-3 and C-4 positions of the phenyl ring linked to oxadiazole (–OCH_3, –OH, –CH_3) showed moderate inhibition activity against both the targets, while substitution of EWGs (–Cl, –NO_2, –CN, –F) showed moderate to excellent inhibition potential. The compound **9d**, with a chloro group in the para position of the terminal phenyl ring was the most active derivative in the test series with the highest COX-2 selectivity with selectivity index of 133.59. The compounds **9d** and **9f** with chloro derivatives at the C-2 and C-4 positions of terminal phenyl showed greater selectivity for the COX-2 enzyme, suggesting that the chlorinated compounds at those positions had significant anti-inflammatory properties. The derivative **9f** with disubstitution of EWGs –4-Cl-3-NO_2 showed moderate enzyme inhibition while **9i** with disubstitution of -Cl at C-2 and C-3 positions exhibited the increased inhibitory potential of the compound against COX-2 enzyme. Similarly, **9g** with the –NO_2 group at the C-4 position exhibited more inhibitory activity against COX-2 and 5-LOX enzymes, respectively, in comparison to **9m** with 2–NO_2 substitution.

5.2.3.3. In vitro enzyme kinetics study

The *in vitro* enzyme kinetics study was conducted to investigate the binding mechanism for compound **9d** against COX-2 enzyme. The Lineweaver-Burk approach was used to plot the graph for three different concentrations of the test compound **9d** against increasing concentrations of substrate, arachidonic acid. The graph showed increased K_m

and unchanged V_{max} with increasing concentrations of compound **9d**, also there was no change in V_{max} for control (no inhibitor), depicting competitive inhibition for COX-2 enzyme. The Dixon plot has been plotted and the outcome indicated that compound **9d** has Ki = 0.22 µM (Figure 5. 18).

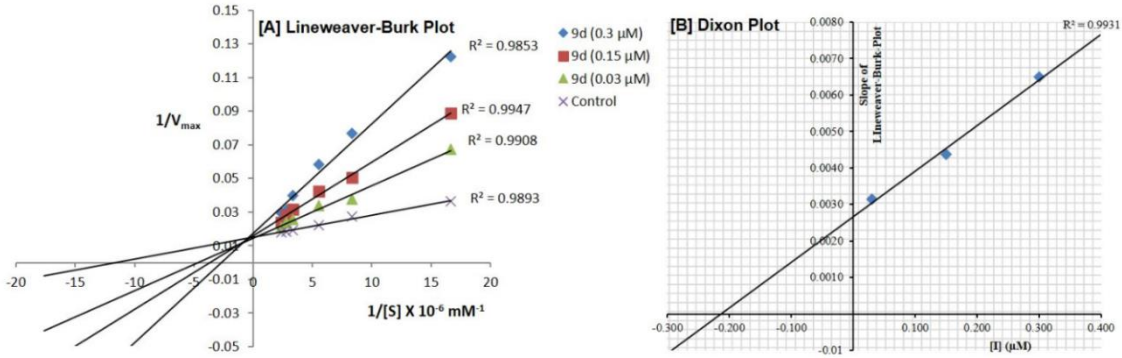

Figure 5. 18. Enzyme kinetics of compound **9d** against COX-2: [A] The Lineweaver-Burk displays competitive inhibition; [B] Dixon plot with Ki at the negative x-axis intersection point.

5.2.3.4. Pharmacological Evaluation

5.2.3.4.1. Acute oral toxicity

The acute oral toxicity assessment was performed on healthy female Wistar rats following the OECD 423 guidelines. The compounds **9d** and **9g** were well-tolerated up to a dose of 500 mg/kg and exhibited no detrimental effects. Also, no mortality was observed even after 14 days, indicating a significant safety margin. Thus, compounds can be examined by additional *in vivo* investigations. The efficacy of compounds **9d** and **9g** was further validated through the histological study of the kidneys, liver, lungs, and heart (Figure 5.19). Compounds **9d** and **9g** exhibited normal histology, which is similar to the control group, indicating no organ damage or detrimental consequences. This validates the compounds' safety profile and establishes their therapeutic properties.

The institutional animal ethical committee authorized the research procedure **(Approval no. IIT(BHU)/IAEC/2023/019)**

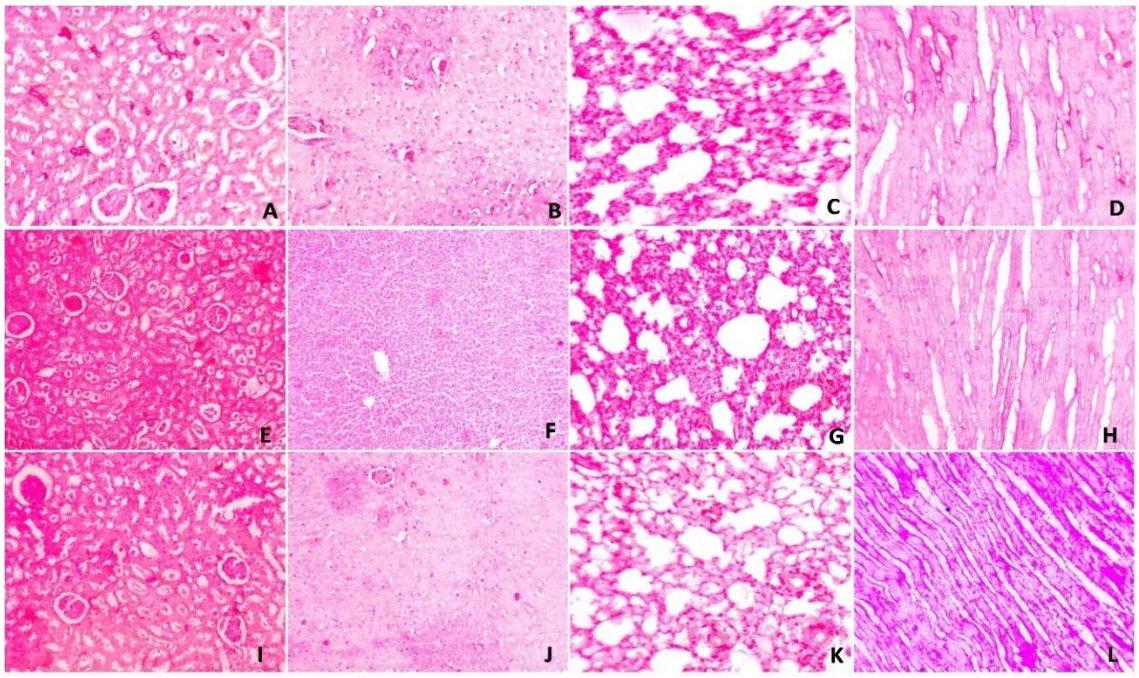

Figure 5.19. A, B, C, D showing normal histopathology of kidney, liver, lung, and heart of control group; E, F, G, H and I, J, K, L showing normal histopathology of kidney, liver, lung, and heart of compound **9d** and **9g** respectively, at the dose of 500mg/kg.

5.2.3.4.2. Carrageenan-induced rat paw edema model

Carrageenan-induced paw edema is a standard exploratory model for assessing the anti-inflammatory effect of different compounds. Carrageenan injected locally into the sub-plantar region of the rat paw causes a severe inflammatory response visible within 30 minutes. Carrageenan-induced paw edema occurs in two stages; wherein the pro-inflammatory histamine, kinins, and serotonin are released in the early stage (around 1h), followed by the release of prostaglandins, free radicals and pro-inflammatory cytokines in the delayed stage (3h post-treatment) {Sadeghi, 2011 #199}. The results of the anti-inflammatory effects of the compounds **9d** and **9g** are presented in Table 5.9. In comparison to the standard drug indomethacin (Indo 10), the investigated compounds markedly reduce paw edema. The anti-inflammatory effect peaked at 5h, indicating the compound's ability to inhibit prostaglandin release in the late stage.

Table 5.9. Carrageenan-induced paw edema

	Swelling thickness in mm						
	0 h	**1 h**	**2h**	**3 h**	**4 h**	**5 h**	**6 h**
Control	3.48 ± 0.21	8.47 ± 0.25	8.65 ± 0.53	8.56 ± 0.45	8.36 ± 0.78	8.47 ± 0.32	8.33 ± 0.42
Indo 10	3.37 ± 0.23	3.74 ± 0.23[a]	3.73 ± 0.26[a]	3.38 ± 0.19[a]	3.14 ± 0.26[a]	3.17 ± 0.26[a]	3.29 ± 0.11[a]
9d (5 mg/kg)	3.51 ± 0.19	6.18 ± 0.54[a,b]	5.63 ± 0.48[a,b]	4.67 ± 0.38[a,b]	4.18 ± 0.45[a]	3.98 ± 0.45[a]	4.14 ± 0.35[a]
9d (10 mg/kg)	3.21 ± 0.14	5.15 ± 0.49[a,b]	3.96 ± 0.51[a,b]	3.47 ± 0.29[a,b]	3.32 ± 0.47[a]	3.29 ± 0.26[a]	3.37 ± 0.31[a]
9d (20 mg/kg)	3.43 ± 0.18	5.12 ±0.32[a,b]	4.11 ± 0.23[a,b]	3.41 ± 0.35[a,b]	3.22 ± 0.39[a]	3.24 ± 0.19[a]	3.41 ± 0.35[a]
9g (5 mg/kg)	3.59 ± 0.24	5.74 ±0.53[a,b]	5.25 ±0.47[a,b]	4.87 ± 0.41[a,b]	4.57 ± 0.43[a,b]	4.22 ± 0.31[a]	4.14 ± 0.31[a]
9g (10 mg/kg)	3.44 ± 0.27	5.32 ±0.41[a,b]	4.55 ±0.36[a,b]	4.41 ± 0.22[a,b]	3.88 ± 0.56[a,b]	3.76 ± 0.42[a]	3.89 ± 0.28[a]
9g (20 mg/kg)	3.65 ± 0.18	5.16 ±0.52[a,b]	4.78 ±0.43[a,b]	4.54 ± 0.34[a,b]	4.32 ± 0.49[a,b]	3.96 ± 0.23[a]	3.91 ± 0.31[a]

The statistics are displayed as mean ± SD; The control group was administered with 0.3% Na CMC solution (10 ml/kg/p.o.) in distilled water. The standard group was given indomethacin (Indo 10) at the dose of 10 mg/kg, p.o. in 0.3% Na CMC. The test compounds **9d** and **9g** were given in doses 5 mg, 10 mg, and 20 mg/kg, p.o. in 0.3 % Na CMC; [a]$p < 0.05$ vs. control; [b]$p < 0.05$ vs. Indo 10.

5.2.3.4.3. Effect on prostaglandin E_2 (PGE_2)

PGE_2 inhibition is reported to be a successful approach to inflammation therapy (Mohassab, Hassan et al. 2021). NSAIDs suppress inflammation by decreasing the production of prostanoids, mainly PGE_2. PGE_2 activates more during inflammatory conditions, thus the inhibition of specific PGE_2 is another approach to subside the adverse effects of NSAIDs. Herein, we have performed an assay to evaluate the PGE_2 inhibition efficiency of the promising derivatives, **9d** and **9g**. The results (Figure 5.20) indicated that **9d** and **9g** markedly inhibit PGE_2 in a dose-dependent manner. This dose-dependent response demonstrates their potential as effective anti-inflammatory therapies, as PGE2 is a crucial mediator in inflammation pathways.

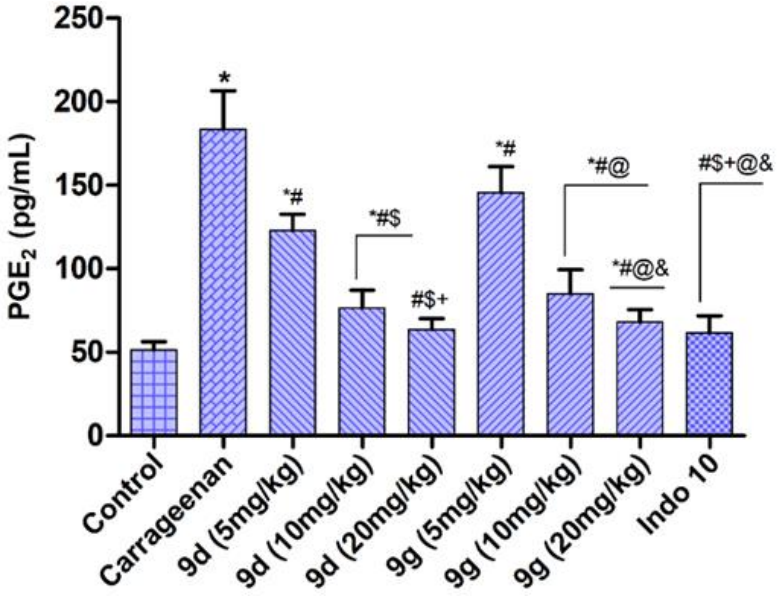

Figure 5.20. Rat paw tissue concentration of PGE_2 for compounds **9d** and **9g** at 5mg, 10mg, and 20mg/kg, p.o.; Data presented in the mean ± SD. *p<0.05 vs Control; #p<0.05 vs Carrageenan; $p<0.05 vs 9d (5mg/kg); +p<0.05 vs 9d (10mg/kg); @p<0.05 vs 9g (5mg/kg); &p<0.05 vs (9g 10mg/kg); (Tukey's test is carried out following the repeated measure one-way ANOVA).

5.2.3.4.4. Effect on cytokines levels

Pro-inflammatory cytokines have been linked to inflammation and are implicated in chronic inflammatory diseases. The decrease in the levels of interleukin-6 (IL-6), and tumor necrosis factor-α (TNF-α) lowers the chances of cardiovascular toxicity and an increase in the level of interleukin-10 (IL-10) presented promising anti-inflammatory activity (Stenvinkel, Ketteler et al. 2005, Liebregts, Adam et al. 2007, Zhang, Cui et al. 2021). The ongoing investigation involved the measurement of IL-6, TNF-α, and IL-10 concentrations from paw tissue samples collected from rats that were treated with indomethacin, and test compounds **9d**, and **9g**, respectively (Figure 5.21). The examined compounds showed a substantial decrease in concentrations of IL-6 and TNF-α. Compound **9d** was the most active among the tested compounds with an IL-6 and TNF-α inhibition in a manner comparable with the standard drug indomethacin. Also, there is

an increase in IL-10 levels indicating the anti-inflammatory activity of the tested compounds.

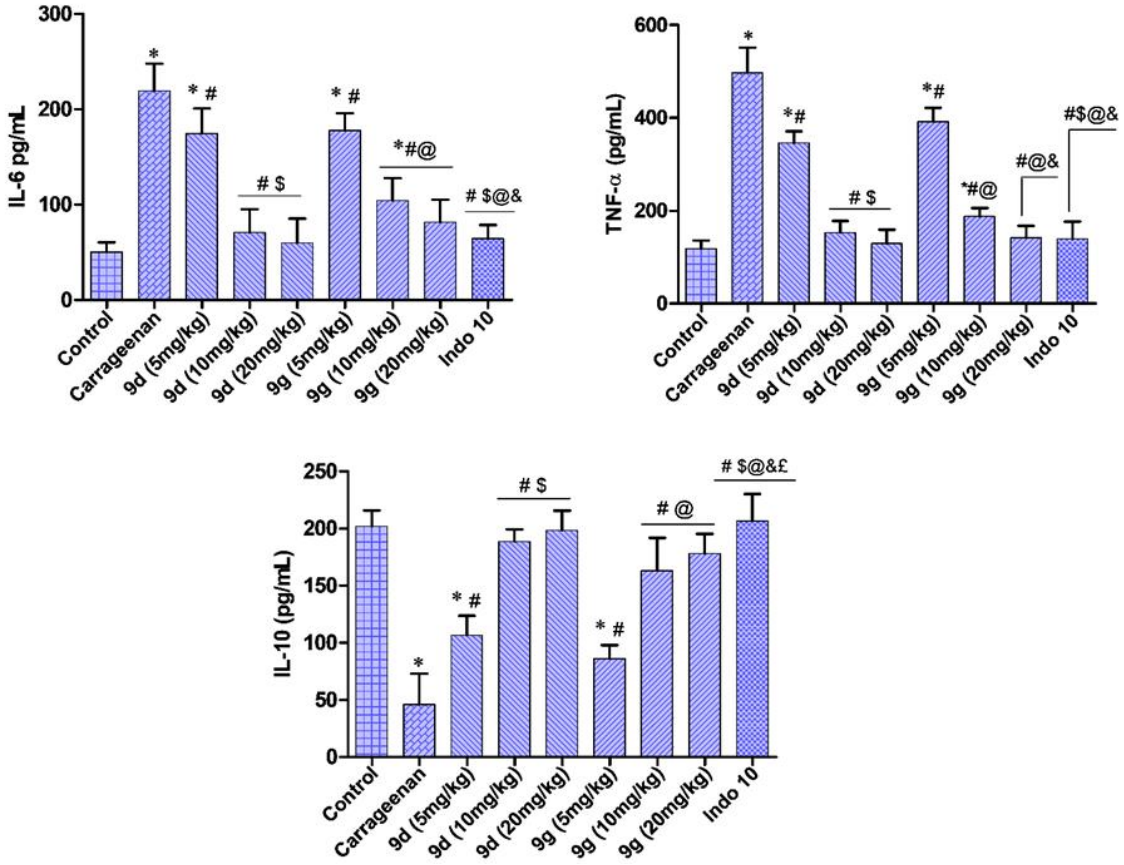

Figure 5.21. Rat paw tissue concentrations of IL-6, TNF-α, and IL-10 for compounds 9d and 9g at 5mg, 10mg, and 20mg/kg, p.o.; Data presented in the mean ± SD. *p<0.05 vs Control; #p<0.05 vs Carrageenan; $p<0.05 vs 9d 5mg/kg; @p<0.05 vs 9g 5mg/kg; &p<0.05 vs 9g 10mg/kg; £p<0.05 vs 9g 20mg/kg; (Tukey's test is carried out following the repeated measure one-way ANOVA).

5.2.3.4.5. Arachidonic acid-induced rat paw edema model

The arachidonic acid injection into the rat's hind paws causes an abrupt and persistent inflammatory response that is inhibited by dual COX/LOX inhibitors and corticosteroids, but not by selective COX inhibitors. The phlogistic activity of LTs renders this model valuable for investigating anti-inflammatory drugs with mechanisms different from that of COX inhibitors (DiMartino, Campbell et al. 1987). A sub-plantar injection of AA produced substantial edema within 30 minutes and hit a peak at 60 minutes. The findings

of this study (Table 5.10) suggested that the compounds **9d** and **9g** mediate its effects by blocking both COX and LOX inflammatory pathways.

Table 5.10. Arachidonic acid-induced paw edema

Groups	Dose	Mean ± SD	% Protection
Control	10ml/kg	6.51 ± 0.37	0
Zileuton	10mg/kg	1.79 ± 0.31	72.59
Celecoxib	10mg/kg	3.39 ± 0.18	47.95
9d	5mg/kg	2.86 ± 0.26	56.12
	10mg/kg	2.01 ± 0.20	69.22
	20mg/kg	1.94 ± 0.34	70.21
9g	5mg/kg	2.92 ± 0.20	55.22
	10mg/kg	2.30 ± 0.33	62.33
	20mg/kg	2.24 ± 0.29	64.36

5.2.3.4.6. Ulcerogenic risk assessment

Compounds **9d** and **9g**, which have significant anti-inflammatory properties, were investigated for ulcerogenic potential in the *in vivo* rat model. The experimental animals were sacrificed and their stomachs were examined for ulcerogenic effects (Table 5.11). The examination showed that the evaluated compounds depicted excellent GI safety profiles with ulcer index of 1.87 and 9.37 for **9d** and **9g**, respectively, at 20 mg/kg dosages, p.o. Conversely, the rats who received indomethacin suffered severe stomach ulcers with an ulcer index of 304.16 and perforations across their stomachs. The indomethacin group displayed an ulcer score of 3.04 ± 0.42 indicating severe mucosal lesions. These findings, along with the histological evaluation of gastric mucosa, provide additional evidence of impressive gastric tolerance of the synthesized compounds in

comparison to indomethacin (Figure 5.22). The absence of inflammation or ulceration highlights the compounds' potential for improved therapeutic properties, especially for the treatment of chronic inflammatory disorders which demand long-term dosing. The results indicate that the synthesized compounds may provide safer, more acceptable alternatives for inflammation management, improving adherence among patients and long-term treatment outcomes.

Table 5.11. Assessment of ulcerogenic liability of Indomethacin, 9d, and 9g

Compound	Dose	Ulcer score	Ulcer Index	Ulceration %
Control	10 ml/kg	0	0	0
Indo 10	10 mg/kg	3.041 ± 0.42	304.16	100
9d	5 mg/kg	0	0	0
	10 mg/kg	0.020 ± 0.01	2.083	1.38
	20 mg/kg	0.018 ± 0.050	1.875	1.25
9g	5 mg/kg	0.010 ± 0.005	1.041	0.667
	10 mg/kg	0.031 ± 0.009	3.125	4.85
	20 mg/kg	0.093 ± 0.010	9.37	4.86

The statistics are displayed as mean ± SD; Control group: 10ml/kg/p.o dose of 0.3% Na CMC in distilled water, Indomethacin group: Indo 10, 10mg/kg/p.o dose in 0.3% Na CMC; The synthesized compounds **9d** and **9g** were administered in doses 5mg, 10mg, and 20mg/kg, p.o. in 0.3 % Na CMC.

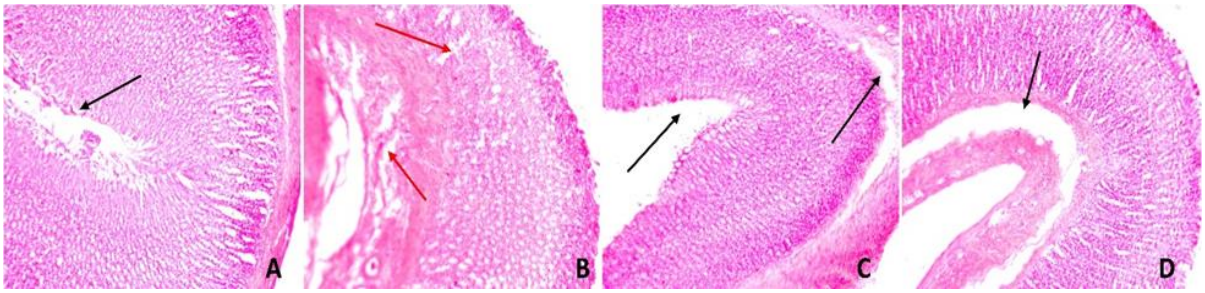

Figure 5.22. Gastric mucosa histology photomicrographs (10X): A, showed the control rat gastric mucosa with naturally aligned gastric pits as indicated by black arrow; B, displayed the indomethacin-treated rat group with ulceration-induced exudation of surface epithelium (red arrows); C & D displayed the test compound **9d** and **9g** treated rat's gastric mucosa showing normal mucosal architecture (black arrows).

5.2.3.4.7. Biochemical analysis

Reactive oxygen species (ROS) possess a tendency to aggravate inflammatory responses (Ranneh, Ali et al. 2017). To investigate if oxidative stress contributes to gastric mucosal damage, the glutathione (GSH) levels, Superoxide dismutase (SOD), and nitrite have been examined and results were presented in Figure 5.23. A significant variation in oxidative stress was observed in the stomach tissues of indomethacin and the control groups. The compound **9d** demonstrated substantial efficacy in enhancing antioxidant activity compared to **9g** and the standard drug indomethacin.

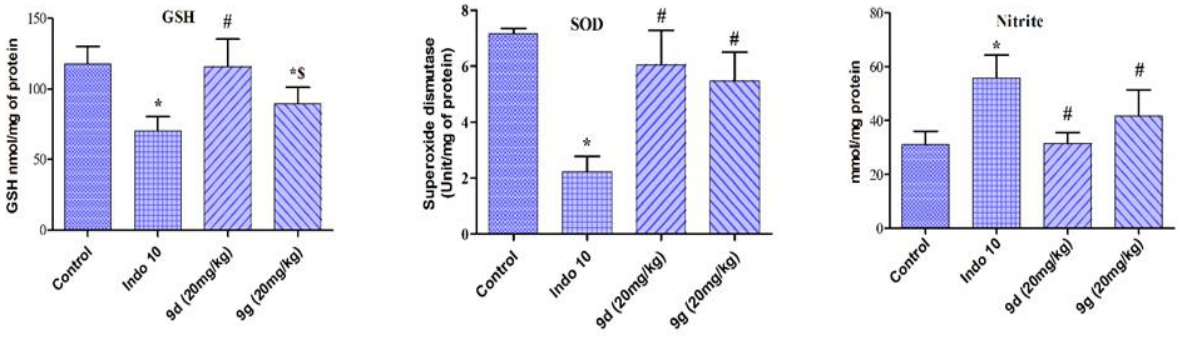

Figure 5.23. The statistics are displayed as mean ± SD; rats (n = 6)/group; *p < 0.05 vs Control (0.3 % sodium CMC mixture in distilled water; 10 ml/kg given orally); #p < 0.05 vs Indo 10 (10 mg/kg given orally) in 0.3 % sodium CMC solution; $p<0.05 vs **9d** 20mg/kg (Tukey's test is carried out following the repeated measure one-way ANOVA)

5.2.3.4.8. Assessment of liver and kidney functions

NSAIDs have been associated with drug-induced liver and kidney toxicity. Compounds **9d**, **9g,** and indomethacin were tested for their effects on the livers of rats using the serum biomarkers alanine aminotransferase (ALT) and aspartate aminotransferase (AST). Both ALT and AST levels were increased in the indomethacin-treated group, while there was no significant difference between the control group and the synthesized derivatives group. They were also checked for kidney function of rats; the indomethacin group showed higher levels of creatinine and urea while the synthesized derivatives had a non-significant difference from the control group, indicating the renal safety of the novel

compounds The results of estimating these biochemical markers validated the relative safety of synthesized derivatives in comparison to the standard drug (Figure 5.24).

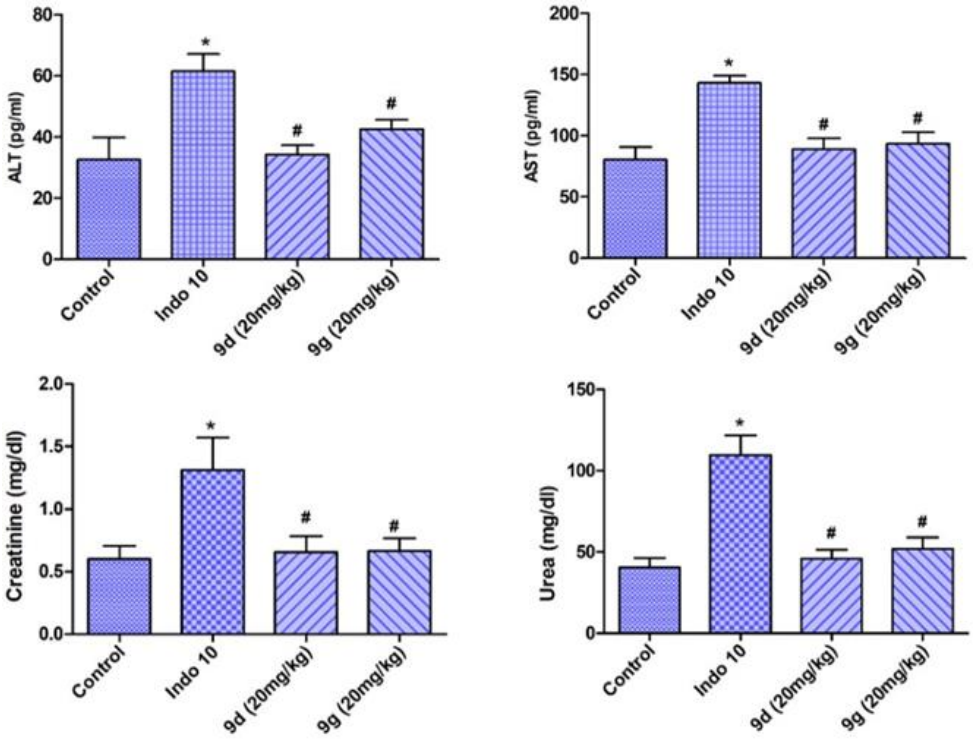

Figure 5.24. The measurement of ALT, AST, creatinine, and urea in the serum of rats treated with standard indomethacin (Indo 10), **9d,** and **9g**. The statistics are displayed as mean ± SD; rats (n = 6)/group; *p < 0.05 vs Control (0.3 % sodium CMC mixture in distilled water; 10 ml/kg given orally); #p < 0.05 vs Indo 10 (10 mg/kg given orally) in 0.3 % sodium CMC solution; (Tukey's test is carried out following the repeated measure one-way ANOVA)

5.2.3.4.9. Effect on platelet aggregation

Inflammation induces vascular injury and recruits platelets by adhering to injured subendothelial cells resulting in the accumulation of platelets. Platelet activation releases multiple platelet aggregating agents, including adenosine diphosphate (ADP), which exacerbates platelet aggregation and causes secondary myocardial tissue damage (Ramakrishna and Krishnamurthy 2023). To discover the role of compounds **9d** and **9g** in the production of platelets, we conducted a platelet aggregation assay. The results of the study showed that the treatment with compounds **9d** and **9g** reduces platelet aggregation (Figure 5.25).

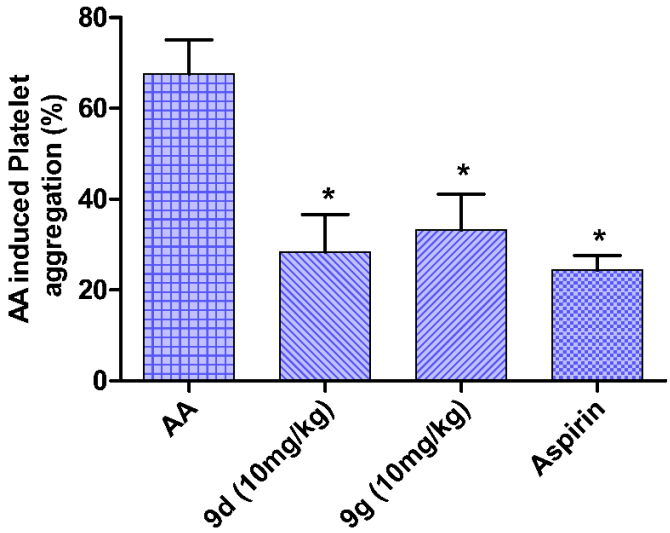

Figure 5.25. The statistics are displayed as mean ± SD; rats (n = 6)/group; *p < 0.05 vs AA; (Tukey's test is carried out following the repeated measure one-way ANOVA)

5.2.3.4.10. Assessment of cardiotoxic liability

5.2.3.4.10.1 Lactate dehydrogenase (LDH) and Creatine kinase-MB (CK-MB)

The present study was designed to investigate the cardiotoxic liabilities of the compounds **9d** and **9g** in Wistar rats. The presence of enzymes LDH and CK-MB in serum indicates myocardial damage. The isoproterenol-induced myocardial infarction model was used to develop myocardial damage in rodents (Banerjee, Das et al. 2016, Philoppes, Abdelgawad et al. 2023). The rats treated with isoproterenol (ISO) had significantly elevated levels of serum LDH and CK-MB, whereas the rats treated with celecoxib did not exhibit a significant difference in serum LDH and CK-MB levels. Notably, compounds **9d** and **9g** significantly reduced LDH and CK-MB levels as compared to the ISO group, suggesting that they protect against ISO-induced myocardial injury. This reduction emphasizes the ability of **9d** and **9g** to reduce cardiac damage, probably owing to their anti-inflammatory and COX-2 selective inhibitory activities, highlighting their therapeutic promise (Figure 5.26).

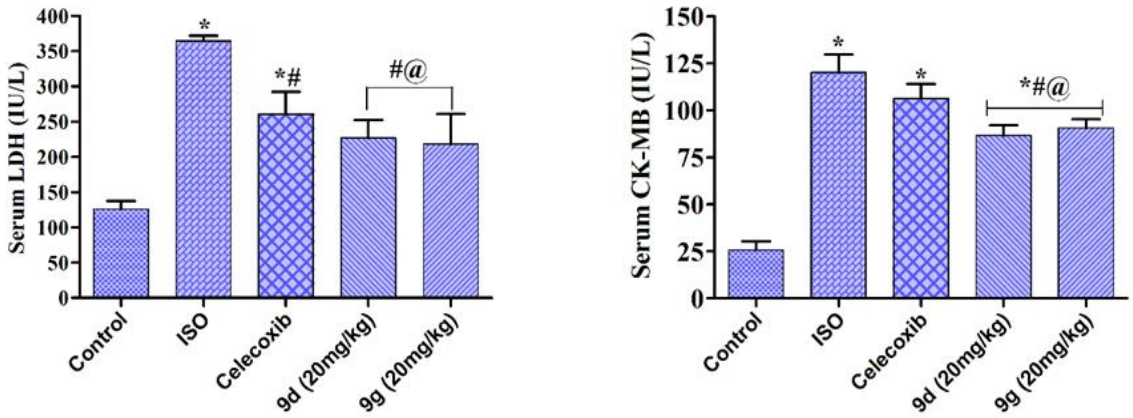

Figure 5.26. The measurement of LDH and CK-MB in the serum of rats treated with isoproterenol (ISO), celecoxib, **9d**, and **9g**. The statistics are displayed as mean ± SD; n = 6 rats per group; *p < 0.05 vs Control (0.3 % sodium CMC mixture in distilled water; 10 ml/kg given orally); $^{\#}$p < 0.05 vs ISO (100 mg/kg given s.c.) in 0.3 % sodium CMC solution; $^{@}$p < 0.05 vs ISO + Celecoxib (10 mg/kg given orally); (Tukey's test is carried out following the repeated measure one-way ANOVA).

5.2.3.4.10.2. Cardiac troponin-I (cTn-I)

Cardiac troponin-I (cTn-I) is yet another marker of drug-induced cardiac cell rupture, leading to enzyme leakage into the bloodstream. The increased troponin level has been reported in the serum of celecoxib-treated groups (Ahmad, Panda et al. 2018), which is consistent with the results of the present findings. The loss of membrane integrity due to myocytes injury might be the reason for troponin release which is indicative of coronary diseases. When compared to the celecoxib group, both **9d** and **9g** showed lower levels of cTn-I, indicating that they did not exacerbate the existing condition, thus suggesting the absence of cardiotoxicity in test compounds (Figure 5.27).

Rats were randomly chosen from each experimental group to investigate cardiac tissue histology and sacrificed. The histological examination of cardiac tissues of rats administered the compounds **9d** and **9g** displayed architecture similar to those found in the control group, with no evidence of cell damage, inflammation, or necrosis (Figure 5.28). This similarity demonstrates that these compounds do not cause toxicity or detrimental changes in cardiac tissues, regardless of testing conditions.

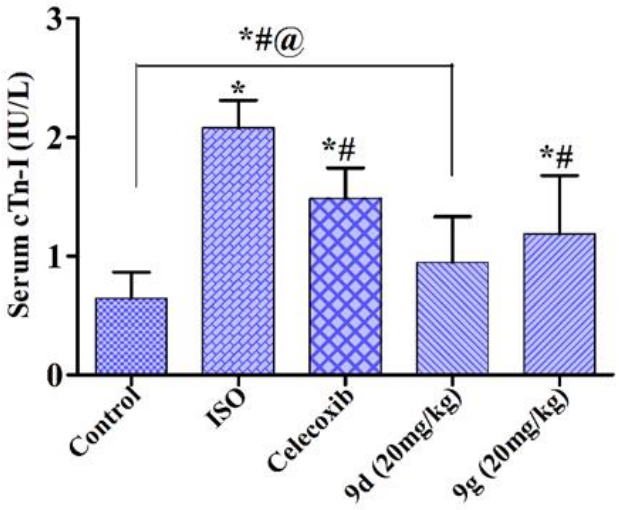

Figure 5.27. The measurement of cTn-I in the serum of rats treated with isoproterenol (ISO), celecoxib, **9d**, and **9g**.The statistics are displayed as mean ± SD; n = 6 rats per group; *p < 0.05 vs Control (0.3 % sodium CMC mixture in distilled water; 10 ml/kg given orally); $^{\#}$p < 0.05 vs ISO (100 mg/kg given s.c.) in 0.3 % sodium CMC solution; $^{@}$p < 0.05 vs ISO + Celecoxib (10 mg/kg given orally); (Tukey's test is carried out following the repeated measure one-way ANOVA).

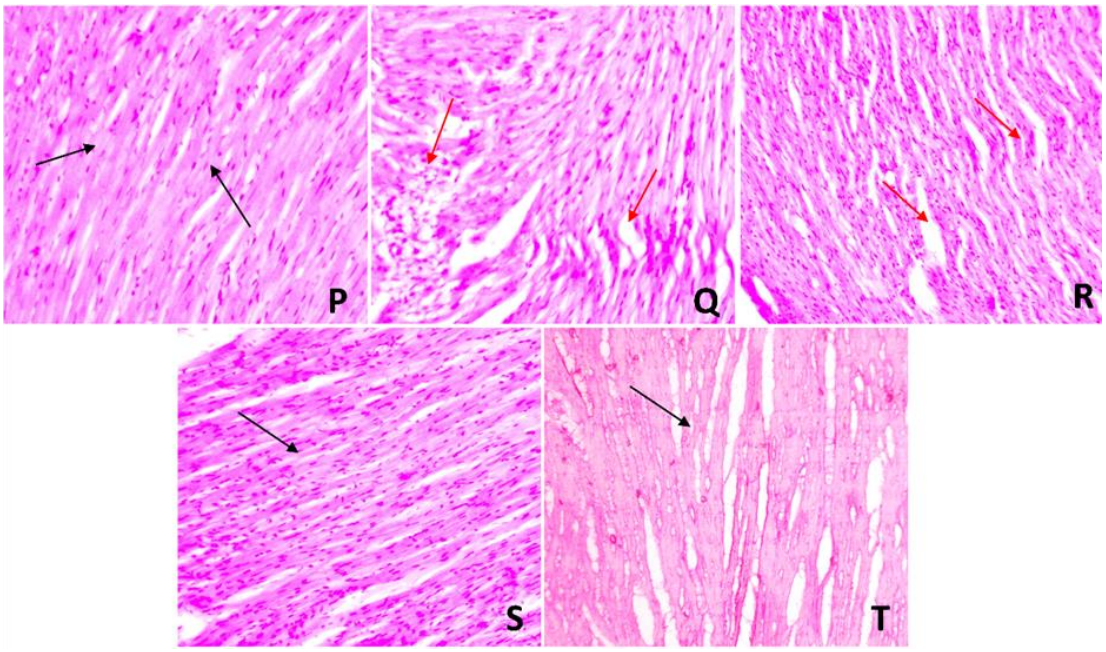

Figure 5.28. Microscopic evaluation of rat heart tissues (H & E staining): P, display control group with well-organized tissues and nuclei; Q, physiology of heart of rats treated with isoproterenol (red arrows) showing portion of damaged tissues and dislocated nuclei; R, displaying the celecoxib group with minor damage to the heart tissues; S & T, showed the promising derivative **9d** and **9g** with normal tissue framework and well-organized nuclei.

5.2.3.4.11. Assessment of analgesic activity

The writhing test has been performed to evaluate the analgesic activity of the promising derivatives. The acetic acid is used to induce pain of peripheral origin. Acetic acid is believed to function indirectly by stimulating endogenous mediators, which activate nociceptive neurons susceptible to NSAIDs and narcotics (Banerjee, Das et al. 2015). In this study (Table 5.12), compound **9d** exhibited a greater percentage of pain inhibition than the standard group indomethacin. The compound **9d** with a dose of 20 mg/kg had 17.83 ± 1.94 writhes and the percentage of pain inhibition (55.78 ± 4.81%), which is close to the standard indomethacin producing 16.50 ± 1.87 writhes and 59.09 ± 4.63% pain inhibition. The test compound **9g** produced 20.33 ± 2.16 writhes and 49.58 ± 5.35% pain inhibition. These findings indicate the efficacy of molecules **9d** and **9g** as analgesic drugs, with pain inhibition similar to the conventional medication indomethacin. The robust performance of **9d**, in particular, emphasizes its potential as a powerful pain management alternative. These findings establish **9d** and **9g** as possible options for additional research and clinical testing in the management of pain.

Table 5.12. Assessment of analgesic activity

Group	No. of writhes (30 min.)	% Pain inhibition
Control	40.33 ± 3.01	0
Indo 10	16.50 ± 1.87	59.09 ± 4.63
9d	17.83 ± 1.94	55.78 ± 4.81
9g	20.33 ± 2.16	49.58 ± 5.35

The statistics are displayed as mean ± SD; Control group: 10 ml/kg/p.o dose of 0.3% Na CMC in distilled water, Indomethacin group: Indo 10, 10 mg/kg/p.o dose in 0.3% Na CMC; The investigated compounds **9d** and **9g** were administered in doses of 20 mg, p.o. in 0.3 % Na CMC.

5.2.3.5.In vitro anti-cancer activity

Inflammation has evolved into an emerging hallmark of cancer. Multiple research findings indicated that dual COX-2/5-LOX inhibitors have anti-proliferative characteristics (Goossens, Pommery et al. 2007, Che, Chen et al. 2016, Aliabadi, Khanniri et al. 2023). The most promising compound **9d** was investigated for its cytotoxic potential against three human cancer cell lines viz A549, COLO-205, and MIA-PA-CA-2 using SRB assay. Adriamycin (ADR), a chemotherapeutic drug often used in anti-cancer therapy, is employed as a reference standard. The finding indicated that compound **9d** possesses substantial anti-cancer properties as shown in Figure 5.29. Compound **9d** demonstrated higher cytotoxic potential against A549 and COLO-205 cell lines, while it showed lesser cytotoxic potential against MIA-PA-CA-2 cancer cell lines (Table 5.13). Compound **9d** demonstrated a high cytotoxic effect against specific cancer cell lines and noteworthy anti-cancer action, suggesting that it is efficient in addressing particular malignancies. These properties make **9d** an appealing option for application in conjunction with cancer therapy regimens, perhaps increasing the effectiveness of preexisting chemotherapeutic medicines such as Adriamycin.

Table 5.13. Cytotoxic potential against A549, COLO-205, and MIA-PA-CA-2 human cancer cell lines

Compound	Cell line	GI50 (μM)
ADR	A549	0.077
	COLO-205	0.0999
	MIA-PA-CA-2	0.002
9d	A549	0.731
	COLO-205	1.22
	MIA-PA-CA-2	2.32

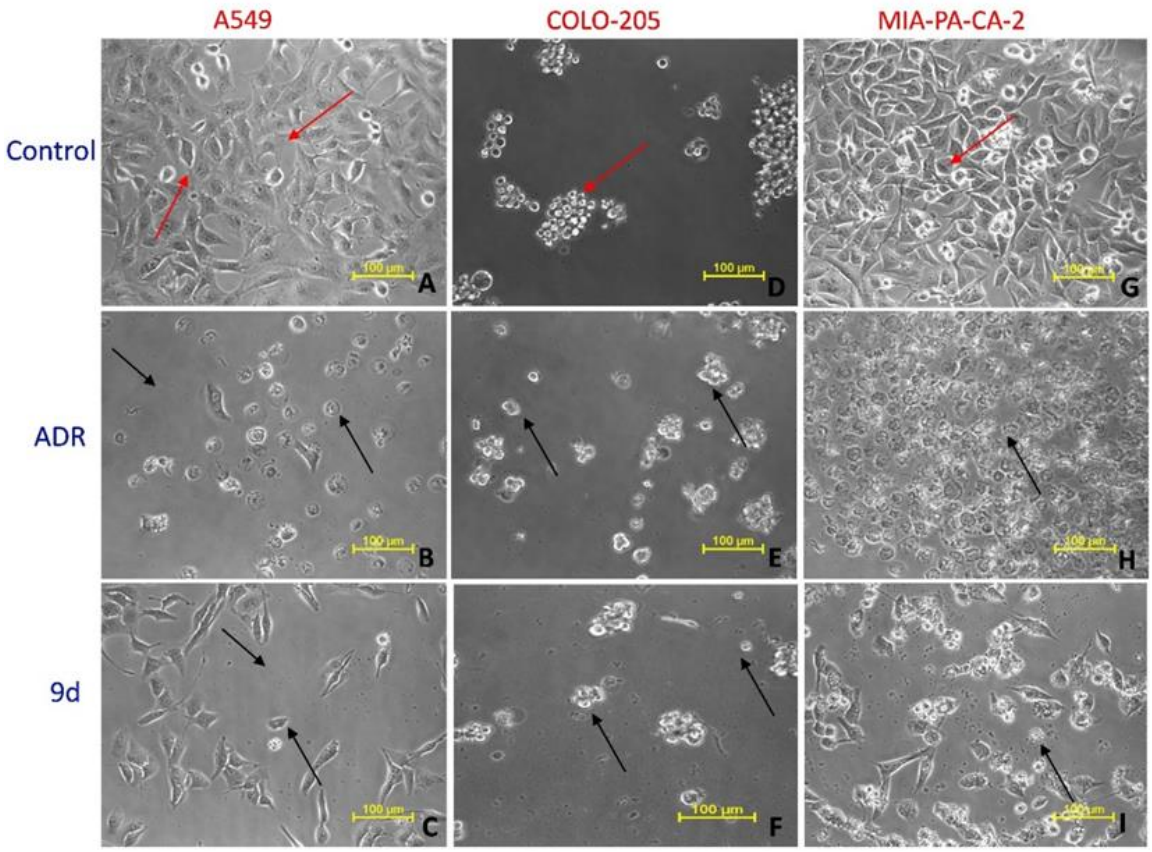

Figure 5.29. Cytotoxic potential of compounds in A549 human lung cancer cell lines **(A, B, C);** COLO-205 human colon cancer cell lines **(D, E, F)**; and MIA-PA-CA-2 **(G, H, I)** human pancreatic cancer cell lines. The control group depicted untreated cancer cell lines, while the ADR group showed the treatment with reference standard, and the **9d** group showed test compound treatment. Red arrows indicated the cancer cells and black arrows indicated the decrease in the number of cancer cells.

5.2.3.6. Anti-cancer activity in in vivo model system

In this study, we examined *in vivo* anti-cancer activity of compound **9d** against the Ras^{V12} induced *Drosophila* Glioblastoma cancer model. Ras overexpression upregulates multiple signalling cascades, inducing inflammatory responses within glial cells, ultimately leading to over-proliferation, tumor formation, and absolute lethality during the early developmental stages of *Drosophila* (Pratyusha, Victoria et al. 2018, Kattan and Hancock 2020, Mukhopadhyay, Vander Heiden et al. 2021, Zhao, Wu et al. 2021). The toxicity assessment and dose determination of compound **9d** was assessed in wild-type

flies to define median lethal dose 50 (LD_{50}). The LD_{50} of **9d** was determined to be 100 µM (Fig. 12). Compound **9d** displayed over 70% fly eclosion rate at 50 µM concentration and 100 µM showed toxicity by reducing the eclosion rate to below 50%. Hence, we screened **9d** against cancer bearing *Ras*^{V12} larvae at safe doses of 10 µM and 50 µM concentrations. In therapeutic experiments, **9d** at 10 µM and 50 µM concentrations significantly rescued 3rd instar larval lethality and enhanced early pupal developmental differentiation as compared to untreated *RasV12-induced* diseased *Drosophila* (Figure 5.32).

5.2.3.6.1. Toxicity Assessment

A comprehensive toxicity study in wild type *Drosophila* resulted in the LD_{50} dose of 100 µM for compound **9d**. At doses of 1 µM and 10 µM, approximately 92% and 84% of flies effectively eclosed, exhibiting minimal toxicity. Also, at 50 µM dose, there was successful eclosion of nearly 71% of F1 flies into adults. However, at doses 100 µM and 200 µM, the flies' eclosion were reduced to 41% and 24% respectively (Figure 5.30).

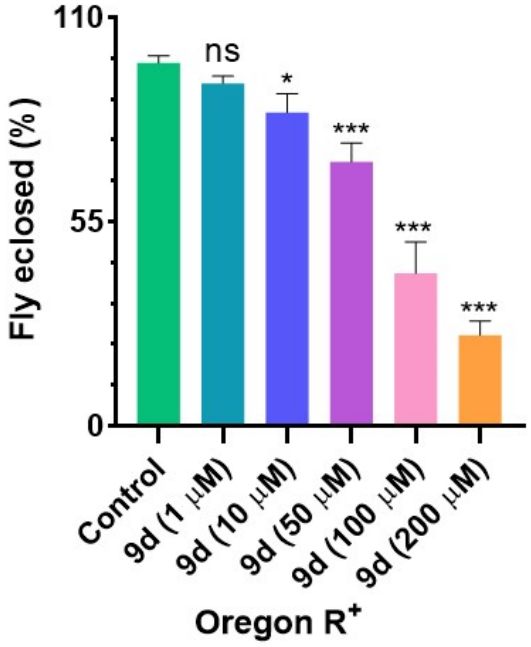

Figure 5.30. Histogram represents the percent of fly eclosed in the untreated control group and 9d treated with 1 µM, 10 µM, 50 µM, 100 µM, 200 µM concentrations. Dunnett's multiple

comparisons test was used to ascribe the significance values. Non significance (ns), p> 0.05, *p < 0.05, and ***p > 0.001

5.2.3.6.2. *In vivo* anti-cancer efficacy

The anti-cancer potential of test compound **9d** was examined by treating Ras^{V12}-induced Glioblastoma cancer. The compound **9d** at 10 µM and 50 µM concentrations resulted in therapeutic efficacy in a dose-dependent manner (Figure 5.31). The study revealed that there was near absolute lethality at the larval stage in the development of cancer bearing larvae, whereas the **9d** treated groups demonstrated significant improvement in larval development to pupal transition. Interestingly, at 10 µM dose, there was a statistically significant improvement in pupal development of **9d** (p = 0.14). Notably, at 50 µM dosage, **9d** showed a significant reduction in 3rd instar larval lethality, increased 3rd instar larval survivability, and transition to early pupal development (p = 0.006). The **9d** treatment at both 10 µM and 50 µM dosages improved 3rd instar larval survivability (p = 0.12 and p = 0.006, respectively) and early pupal survivability (p = 0.007 and p < 0.001, respectively) compared to untreated Glioblastoma cancer bearing larvae as illustrated in Figure 5.32.

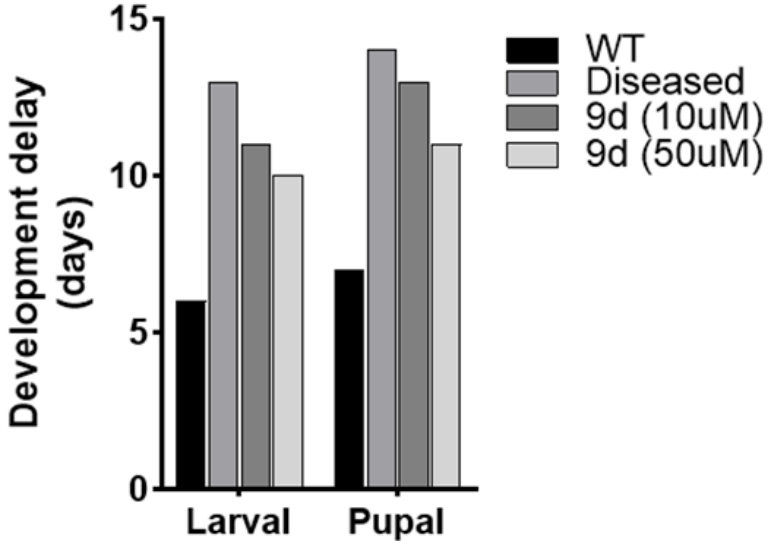

Figure 5.31. Histogram represents percent of fly eclosed in untreated control group and 9d treated with 10 µM, and 50 µM concentrations.

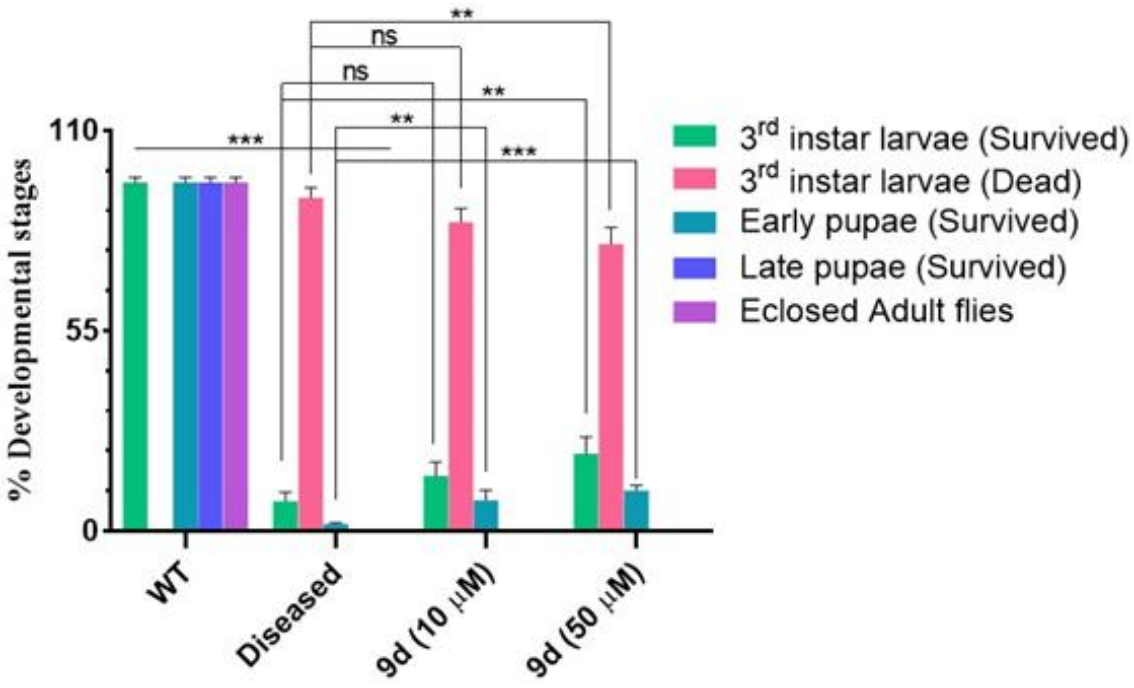

Figure 5.32. Histogram represents the percent of different developmental stages of WT, Diseased (repo-GAL4/ UAS-Ras^{V12}), and diseased treated with 9d treated at 10 µM, and 50 µM concentrations. Tukey's multiple comparisons test was used to ascribe the significance values. Non significance (ns) p> 0.05, *p < 0.05, **p < 0.01, and ***p > 0.001.

5.2.3.7. Pharmacokinetics studies

A primary pharmacokinetic investigation was conducted to ascertain the correlation between the *in-vitro* and *in-vivo* outcomes. The most effective derivative **9d** was administered orally on healthy male Wistar rats at the dosage of 10 mg/kg. Blood samples were taken from the retro-orbital plexus at scheduled times (Figure 5.33). The pharmacokinetic parameters were analyzed using the extravascular non-compartment model to evaluate absorption. distribution, metabolism, and excretion of the test drug. This model is based on direct observation of plasma concentration-time data and does not assume any particular compartmental structure for drug disposal. Key parameters such as the area under the curve (AUC), peak plasma concentration (Cmax), time to peak concentration (Tmax), elimination half-life (t1/2), and clearance (CL) were calculated

and results obtained are shown in Table 5.14.

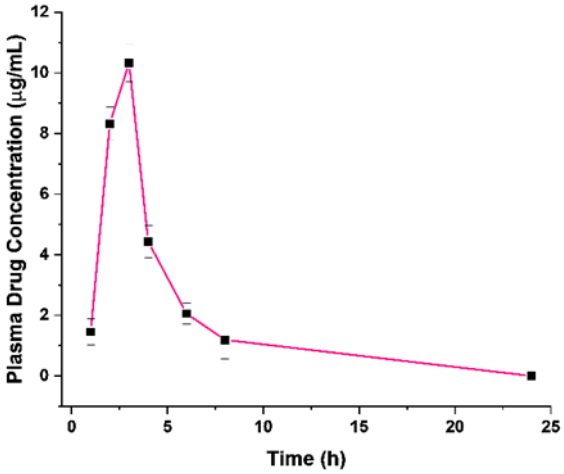

Figure 5.33. The drug release profile of orally administered drug 9d in the rat model.

Table 5.14. Results of pharmacokinetic parameters after oral dosing

Parameters	**Effect of 9d**
C_{max} (µg/ml)	10.32 ± 0.043
T_{max} (h)	3.00 ± 0.554
$(AUC)^{0-24}$ (µg/ml h)	32.06 ± 0.625
$t_{½}$ (h)	2.11 ± 0.053
MRT (h)	3.42 ± 0.0614

*All values are expressed as the mean ±SD (n = 3)